

University of Louisville

ThinkIR: The University of Louisville's Institutional Repository

Electronic Theses and Dissertations

8-2019

SolarPede: An untethered micro robot powered by light.

Jordan Fredrick Klotz
University of Louisville

Follow this and additional works at: <https://ir.library.louisville.edu/etd>



Part of the [Electrical and Electronics Commons](#), [Nanotechnology Fabrication Commons](#), and the [Systems and Communications Commons](#)

Recommended Citation

Klotz, Jordan Fredrick, "SolarPede: An untethered micro robot powered by light." (2019). *Electronic Theses and Dissertations*. Paper 4263.
<https://doi.org/10.18297/etd/4263>

This Master's Thesis is brought to you for free and open access by ThinkIR: The University of Louisville's Institutional Repository. It has been accepted for inclusion in Electronic Theses and Dissertations by an authorized administrator of ThinkIR: The University of Louisville's Institutional Repository. This title appears here courtesy of the author, who has retained all other copyrights. For more information, please contact thinkir@louisville.edu.

SOLARPEDE: AN UNTETHERED MICRO ROBOT POWERED BY LIGHT

By

Jordan Fredrick Klotz
B.S. in EE, University of Louisville, 2018

A Thesis
Submitted to the Faculty of the
J. B. Speed School of Engineering of the University of Louisville
in Partial Fulfilment of the Requirements
for the Degree of

Master of Science in Electrical Engineering

Department of Electrical and Computer Engineering
University of Louisville
Louisville, Kentucky

August 2019

Copyright 2019 by Jordan F. Klotz

All rights reserved

SOLARPEDE: AN UNTETHERED MICRO ROBOT POWERED BY LIGHT

By

Jordan F. Klotz

A Thesis Approved on

July 18, 2019

by the following Thesis Committee

Dr. Dan O. Popa

Dr. Andre J. Faul

Dr. Thad L. Druffel

ACKNOWLEDGEMENTS

I would like to thank Dr. Dan O. Popa for his continued support throughout my undergraduate and graduate research. His teachings inside the classroom and at the lab have been invaluable in my path towards this degree. I would also like to thank Dr. Andre J. Faul whose influence as an instructor helped make this document and degree possible. I want to specially thank Dr. Popa, Dr. Faul, and Dr. Thad E. Druffel for their service as committee members for the review of this thesis.

I am grateful to the Department of Electrical & Computer Engineering as well as the Micro and Nano Technology Center of the University of Louisville for their support and training as a Teaching Assistant. I am also thankful for the sponsorship of Dr. Dan Popa and Dr. Shamus McNamara during my graduate studies. I am especially thankful for the opportunity to join with Next Generation Systems (NGS) research group and for all the skills, knowledge, and friends gained along the way. Because of their feedback and guidance, I have reached more than I thought possible.

I am thankful to my family who raised me to be of good character and strong work ethic. I credit much of my success to the values and core of my teachings while under their care; and I know that, without them, I could not have succeeded to this extent.

Lastly, I would like to thank the National Science Foundation (NSF) for their partnership with NGS which helped foster a genuine and full research experience. I have learned so much during my graduate studies, and ultimately, NSF made it possible.

ABSTRACT

SOLARPEDE: AN UNTETHERED MICRO ROBOT POWERED BY LASER LIGHT

Jordan F. Klotz

May 7, 2019

Micro-Robotics looks to implement robotics principles at a small scale and has gained popularity in recent decades as a gateway to new research areas such as micro-factory applications. The SolarPede is a second-generation, cm-scale micro-crawler designed for such micro factory applications which is equipped with a legged locomotion system and an electronic backpack. The SolarPede is an evolution of its predecessors and features power and signal conditioning capabilities, gait pattern generation, and Bluetooth connectivity. The components which make up SolarPede have been fully validated and tested, and its systems have been realized in the form of a body made from Micro-Electro-Mechanical System (MEMS) actuators and the electronic backpack made from a pair of custom Printed Circuit Boards (PCBs). The body and electronic backpack are connected through gold wire-bonding, and the completed system is programmed using Universal Asynchronous Receiver/Transmitter to the onboard Micro Controller.

This work details the research findings during the design, validation, and fabrication of electronic systems for SolarPede. All testing procedures and experimental setups used in validation are described in this document. The experimental results show

that SolarPede can be powered by white light generated using a solar simulator lamp and that it is capable of holonomic movement of a payload at 13 $\mu\text{m/s}$.

TABLE OF CONTENTS

ACKNOWLEDGEMENTS	iii
ABSTRACT.....	iv
LIST OF TABLES	ix
LIST OF FIGURES	x
CHAPTER 1 INTRODUCTION	1
1.1 Motivation	1
1.2 Contributions	3
1.3 Thesis Organization.....	4
CHAPTER 2 BACKGROUND	6
2.1 MEMS and Microrobotics	6
2.1.1 Microfactories.....	8
2.2 Light Power	9
2.3 Earlier Crawler Designs.....	10
2.3.1 Previous Electronic Backpack Designs	10
2.3.1.1 ARRIPede Version 1.....	10
2.3.1.2 Capstone 2017, ARRIPede Version 2	11
2.3.1.3 Capstone 2018, ARRIPede Version 3	13
2.3.1.4 Independent Study 2018, SolarPede Version 0.....	15
2.3.2 Previous MEMS Layouts.....	17
CHAPTER 3 DESIGN AND MODELLING	19
3.1 SolarPede Current Design	19
3.1.1 Current Electronic Backpack design	19
3.1.1.1 Die Testing Board	21
3.1.2 Current MEMS Layout.....	22
3.2 Modelling	24
CHAPTER 4 FABRICATION AND PART SELECTION.....	26
4.1 Part Selection.....	26
4.1.1 Voltage Booster	26
4.1.2 Transistor Array.....	27
4.1.3 Micro Controller.....	27
4.1.3.1 Communication Protocol	28

4.1.3	Micro Controller Cont.	30
4.1.4	Solar Cell.....	30
4.2	Assembled Backpack.....	31
4.2	Body Fabrication and Packaging.....	32
4.3	MEMS Assembly	34
CHAPTER 5 EXPERIMENTATION AND VALIDATION.....		36
5.1	Set up and Tools	37
5.1.1	Set up for Leg Displacement Experiments	37
5.1.1.1	Set up for Single Leg Experiments	37
5.1.1.2	Multi Leg and Control Strategy	39
5.1.1.3	Setup for Payload Experiments.....	40
5.1.2	Set up for validation of Light Power	42
5.1.2.1	Power Output Validation	42
5.1.2.2	Light Power of The Electronic Backpack	43
5.2	Experimental Results.....	44
5.2.1	Leg Displacement Results	44
5.2.1.1	Single Leg Experiment Results.....	44
5.2.2.2	Multi Leg Test Results.....	47
5.2.2.3	Payload Test Results	48
5.2.2	Solar Test Results	50
5.2.2.1	General Power Output Results	50
5.2.2.2	Solar-Leg Results.....	51
CHAPTER 6 CONCLUSIONS AND FUTURE WORK		52
6.1	Conclusions	53
6.2	Future Work.....	54
REFERENCES		57
APPENDIX A.....		61
APPENDIX B		67
APPENDIX C		70
CURRICULUM VITA		76

LIST OF TABLES

Table 5	19
Table 1	29
Table 2	36
Table 3	46
Table 4	49

LIST OF FIGURES

Figure 1. Shows the ARRIPede V1. Left) Assembled Prototype in “belly up” position. Right) Assembled Prototype in “belly down” position [35].	11
Figure 2. Shows ARRIPede V2. Left) Pads only. Right) Fully Assembled [39].	12
Figure 3. Shows the Eagle Layout of the ARRIPede V2. Top Left) Shows the top face of the Top Board. Top Right) Shows the bottom face of the Bottom Board. Bottom Right) Shows the top face of the Bottom Board. Bottom Left) Shows the bottom face of the Bottom Board [39].	14
Figure 4. Shows the Printed Boards for the ARRIPede V2. Top Left) Shows the top face of the Top Board. Top Right) Shows the bottom face of the Bottom Board. Bottom Left) Shows the top face of the Bottom Board. Bottom Right) Shows the bottom face of the Bottom Board [39].	14
Figure 5. Shows the SolarPede V0. Left) Power Systems Board with castellated through hole connections. Right) RF Digital RFD22301 controller with antenna.	16
Figure 6. Shows ARRIPede V1 MEMS layouts generated using LASI. Left) Shows ARRIPede V1 Belly. Middle) Shows type 1 belly with theoretical omnidirectional movement. Right) Shows type 2 belly intended to add backward movement [36].	17
Figure 7. SolarPede L-Edit mask #1 (ARRIPede) and CAD model [41].	18

Figure 8. SolarPede system diagram. Rounded rectangles indicate a component used in the micro crawler. The arrows show some shared or provided resource and the delivery method. The blue dashed rectangles show on what the component will be mounted. 20

Figure 9. Shows the Die Testing Board for SolarPede V2. It shows the process of attaching of the Die Board to the Base Board from several angles. 21

Figure 10. SolarPede L-Edit mask #2 (omni-directional) and CAD model [41]..... 22

Figure 11. Shows mecanum style wheels with vectors of motion for individual wheels to generate body motion in the direction of the large arrow. 23

Figure 12. Shows current SolarPede body layout with vectors theorized for the replication of the mecanum behavior as shown in Fig. 11. Black arrows indicate a typical actuation of a high frequency while red arrows indicate a lower frequency. A difference in speed between the left or right sides should result in the rotation of the robot in a particular direction. 23

Figure 13. Mass-spring-damper free body diagram for SolarPede [41]. 24

Figure 14. System Diagram showing components as chosen. 31

Figure 15. Shows the final electronic backpack assembled. The board on the left houses the microcontroller and necessary UART connections. The board on the right is the bottom board which contains power components including the voltage booster. 32

Figure 16. Top and Side views of a typical wafer during SOI fabrication of SolarPede. (SiO₂ width made larger for visual). A) Initial SOI wafer. B) Wafer after metal deposition. C) Metals patterned to define traces and contacts. D) Structure after DRIE process E) Final wafer after HF release. 33

Figure 17. NeXus Micro-Assembly System M1) Manipulator with vacuum tipped microgripper on X-Y- θ motorized stage. M2) 6 DOF positioner stage consisting of motorized X-Y-Z- θ and manual X-Y [41]..... 35

Figure 18. SolarPede legs assembled. Left) SolidWorks model of leg with dimensions recorded in Table 1. Right) Actual assembled leg imaged while in M2 of NeXus station [41]..... 35

Figure 19. Single leg testing structure on bread board. Keyence sensor placed in line with this leg for measurement. 38

Figure 20. Left) Assembled Legs under NeXus Imaging System [41]. Right) Legs under camera during “Belly-Up” operation. 40

Figure 21. A: Assembled SolarPede Legs [41]; B: Legs labeled as in program with pairs marked [41]; C: MEMS die wire bonded and in a package with payload resting on top [41]; D: Vectors for payload motion under rotation gait sequence [41]..... 41

Figure 22. Solar cell and light power verification set up. Left) Set up with laptop and SolarPede [41]. Right) Close up of cell and solar simulator..... 43

Figure 23. Shows the experimental setup for the powering of the SolarPede V1 electronic backpack using light emitted from a solar simulator lamp. 44

Figure 24. Shows the average displacement vs power for single leg experiments with legs given full time to extend [41]..... 45

Figure 25. Left) Plot of robot body velocity vs applied voltage for a range of frequencies [41]. Right) Plot of robot body velocity vs applied frequency for a range of voltages [41]. 47

Figure 26. Shows the labelling and pairing of legs for SolarPede. A) Shows the gate sequence with pairs labeled. B) Shows the truth table for the legs to result in leftward motion of the payload. C) Shows the naming conventions of SolarPede legs. 49

Figure 27. The X axis denotes the Solar Simulator input power and the Y axis denotes the output power from solar cell/input to the voltage booster. 51

Figure 28. Shows the SolarPede leg under high resolution camera. 52

Figure 29. Shows the top board and proposed mating Solar Cell. X's mark unconnected terminals which would line up with through-holes shown in the right. The two copper colored holes near the bottom of the proposed board would be connected to ground and power. 54

Figure 30. Shows the final system layout with the Solar Cell. 54

Figure 31. Shows a proposed shorter SolarPede backpack with easier assembly. 55

Figure 32. Shows a theoretical Flexible SolarPede made on bendable PCBs. This board design could be folded as shown on the right. 56

CHAPTER 1

INTRODUCTION

1.1 Motivation

Micro Electro Mechanical Systems (MEMS) are a category of devices with both electrical and mechanical properties that work in tandem and can be tailored towards a variety of specific purposes. In general, they are made through micro fabrication processes [1] [2]. MEMS technology is used for the manufacturing, testing, and operating of small-scale devices with features of micron and sub-micron sizes. Because of the scale of MEMS devices, it can be difficult or even impossible to manipulate them with traditional tools, by hand, or even with tweezers.

Micro robotics often employs MEMS technology to bridge the gap between the micro and macro domains. While micro robotics has been able to apply concepts, theorems, and properties of macro robotics to enable interactions between a human operator and the micro world, there are many challenges which even micro robotics has yet to overcome. For example, there are many forces and behaviors of materials which are not relevant at the macro scale but become a driving element at the micro scale. Stiction for example, is a force which holds little to no bearing on day to day human interactions, but in the micro robotics world, small structures might adhere to surfaces or tools due to this force. Following this same trend, gravity is much less significant to a MEMS device than the molecular forces which bind compounds or nanostructures

together. There are a few approaches to overcoming these properties, but one of the more popular techniques being researched within the MEMS field is top down manufacturing.

The top down manufacturing process helps to remedy the problems that can arise when dealing with a micro system by having one system manufacture or manipulate a slightly smaller system which in turn manufactures or manipulates an even smaller system. This continues under directed assembly until the desired size is achieved. Using this manufacturing model, robust and efficient systems can be created for almost any scale since the devices can be tailored to deal with specific forces or behaviors.

Micro-factory research is a branch of MEMS and Micro Robotics and is one of top down approach to manufacturing systems. Micro factories can create or manipulate nanostructures such as carbon nanotubes and study them under a microscope or with specialized sensors. A user can direct a larger system which is easy to interact with and that system will translate the task to smaller agents. These micro factory systems are an optimization of MEMS manufacturing techniques used for the creation of devices for bio-MEMS, robotics, or sensing.

SolarPede is a micro robot tailored towards micro factory applications in a dry environment. It is envisioned as a mobile manipulator for material handling applications within a micro factory. The holonomic capabilities of SolarPede combined with its potential as a wirelessly powered and controlled micro robot make it ideal for such applications. In the top down manufacturing scheme, SolarPede serves as necessary connection between the user and the product being produced. Because of SolarPede's medium size, it can be manipulated by hand but is also small enough and dexterous

enough to be useful at the micro scale when used in conjunction with other micro factory robots such as ChevBot and sAFAM as shown in [3] and [4] respectively.

1.2 Contributions

The research described in this thesis has made important contribution toward understanding of a class of light-actuated MEMS mobile microrobots including:

- The design of SolarPede, a multi-legged, stick-and-slip, micro crawler consisting of a body fabricated using MEMS technology and an electronic backpack housing printed circuit boards and a solar cell. This novel micro robot is designed for operation in a dry environment, specifically targeting micro factory applications. SolarPede features wireless communication and control, light power, and holonomic mobility on a flat substrate.
- The robot's body was dynamically modelled, and SolarPede's stick-and-slip motion, dynamic control, and power balance in conjunction with a solar simulator were experimentally confirmed. The cm-scale robot was tested in "belly up" conveyor configuration and is shown to be capable of translation of a payload at speeds of up to $13 \mu/s$ in all 2-dimensional translational directions and demonstrating rotational capabilities.
- The SolarPede's gait is generated by multiplexing actuator pairs, which are placed in a 45-degree pattern to enable holonomic motion. Research conducted generated proper gait patterns to generate controlled motions with power generated by a commercial solar cell placed on top of the microrobot.

This research resulted in the publication of the conference paper: Klotz, Jordan; Wei, Danming; Yang, Zhong; Sherehiy, Andriy; Saadatzi, Mohammad N.; Zhang, Ruoshi; Popa, Dan O. “Concept Validation for a Novel Stick-and-Slip, Light-Powered, Mobile Micro-Crawler” in proceedings of Manipulation, Automation, and Robotics at Small Scales (MARSS), 1-5 July, Helsinki, Finland, 2019.

1.3 Thesis Organization

This thesis is organized as follows:

CHAPTER 2 contains background information on technologies and research areas used in the body of work including MEMS, Micro Robotics, Micro Factories, and Solar Power.

CHAPTER 3 details the design and modelling of the SolarPede Micro robot including a study of earlier generations of micro crawlers which have preceded SolarPede. It presents a general system diagram and shows the design goals goal with some insight on the final design to be discussed in CHAPTER 4.

CHAPTER 4 details the fabrication of SolarPede’s body and part selection for the electronic backpack. This section also contains a full explanation of the reasoning for design decisions and specific information on the communication methods used.

CHAPTER 5 is split between experimental setup and experimental results for the fabricated micro robot. In the set-up section are images of the equipment used and a description of the experimental process. In the results section are not only the graphs, charts, and images of results, but also a description of any changes made after the setup.

Both parts of CHAPTER 5 contain information on the challenges faced during experimentation and explain how those challenges were overcome.

In CHAPTER 6 are the conclusions drawn from research and future plans to continue development for SolarPede.

APPENDICES showing circuit diagrams and printed circuit board layouts follow CHAPTER 6. APPENDIX A shows diagrams of SolarPede V1 alongside the ARRIPede V2 and SolarPede V0. APPENDIX B shows portions of datasheets used in the generation of printed circuit board layouts and shows portions of the design files used to make SolarPede. APPENDIX C contains MATLAB code used in the modelling of SolarPede and *smart*BASIC code used in the programming of the control module.

The REFERENCES section contains all of the journal papers, theses, books, and documents referenced explicitly or implicitly throughout the text.

The final section of the document is the CURRICULUM VITA for Jordan Klotz, the sole author of this document.

CHAPTER 2

BACKGROUND

2.1 MEMS and Microrobotics

MEMS is an ever-growing field with applications in both robotics and manufacturing. MEMS devices are made through photo lithography or laser etching and can have features of nanometer scale. MEMS devices are most commonly made on silicon substrates or using polymers such as SU-8, PDMS, Parylene. Mainstream MEMS devices include sensors, microstructures, channels, membranes, or other mechanical structures many of which feature transistors of very small sizes [1] [2].

Within micro fabrication systems is also the area of micro robotics which includes systems like positioners, actuators, and mobile robots. Positioners have been realized by numerous research groups and some of the small-scale positioners are even capable of nanometer precision [5] [6] [7] [8] [9]. Actuators of innumerable sizes and shapes have been created within the last 20 years [10] [11] [12]. These actuators feature a variety of power sources, actuation methods, and end effectors [13]. Each of these manipulators' actuators could work with a mobile robot to perform some sort of task.

Mobile micro robots are divided into subcategories based on whether they are driven in wet or dry environments. As with actuators, the designs for mobile micro robots are innumerable; however, most mobile micro robots are designed for operation in wet environments [14] [15] [16] [17]. This is because within a wet environment, systems are

more easily controlled, and behavior is generally more linear [18]. SolarPede was designed with dry environments in mind, but it can be related to some of the systems designed for wet environments. For example, the *MagMite* robot which operates through stick and slip (the same actuation method which SolarPede uses) which is an actuation method in which during the gait motion of the robot, differences in friction and normal forces cause the robot to slip during excitation and then stick when not being actuated. This results in an inchworm-like motion. This stick-and-slip effect in mobile micro robots is well documented by several research groups [14] [7] and is also utilized in positioners and high precision stages [55].

There have been a few recent results in creating mobile microrobots for dry environments including larger robots comparable in size to SolarPede. Microrobots like I-SWARM [19], Kilobot [20], and Alice [21], cilia-like gated crawlers like [22] [23], and flying robots like the one shown in [24] are a few examples of these mobile robots. These robots tend to be very fast (several mm/s or cm/s), but they tend to have a short battery life like with ARRIPede. Unlike smaller robots such as microspheres or particles, these larger cm scale crawlers have many on board systems which would be better supported through continuous power this is often achieved through a tethered system such as with Harvard University's Robobee and ARRIPede. However, this continuous powering of a robot can also be achieved through light or solar power such as through a laser.

There are few light powered robots like I-SWARM [19], [25], [26], and [27]. Assuming power can be delivered to the micro robot system through light, new challenges arise including the selection of the wavelength of light, the efficiency, and the spot size. The spot size is particularly important because the smaller spot size means

increased light intensity, but it makes the tracking of the robot particularly difficult as with Chevbob [3]. For this research, experiments were done with white light and on a fixed target. Further research with SolarPede would have to include tracking or even a shutter system to turn the light on and off for maximum efficiency.

While SolarPede can draw on these past works to a degree, it is very unique in its construction. SolarPede includes all systems onboard including control, gait, and power balance. The robot is at the forefront of its field and falls into a category on its own.

2.1.1 Microfactories

Microfactories are generally theoretical concept that combine many aspects of macro manufacturing to a small scale. These systems are designed to overcome the challenges of directed assembly for objects of small scales [28]. There are many visions for micro factories which are of desktop size [29] [30] [31]. These factories seek to accomplish the assembly and manufacture of nanowires and structures and are a gateway to a top down manufacturing system [32] [33].

Future micro-factory applications require miniaturized mobile and fixed microrobots as envisioned by several research groups in recent work [34] [35]. Within a micro factory, mobile micro-robots will be needed to reposition material in the micro-factory while being capable of wireless navigation and autonomous task execution [34].

2.2 Light Power

Energy taken from light is a highly desirable form of power as it is both clean and renewable. Furthermore, if conditions are artificially maintained, it can serve as an endless power supply for continuous operation of a system without the use of a battery. The use of a solar simulator lamp allows for applications of solar powered devices in a highly controlled environment without a dependence on time of day or external factors. More specifically, a type of solar simulator called a Xenon Arc lamp is available for use. This lamp uses Xenon gas to generate white light similar in nature to the light provided by the sun. This light is capable of delivering power at a distance which can be harnessed by a solar cell.

Light power has seen recent application in micro robotics as discussed above with Harvard's Robofly [23], an untethered version of the previous RoboBee, and a relatively new robot from the University of Pennsylvania and Cornell University [26]. Some challenges can arise with using light power for continuous powering of a robot. This can be difficult for several reasons. Firstly, a continuous light source generates a lot of heat, so pulses are often required. Secondly, keeping the light centered on a moving target can be quite difficult as with RoboFly [23] and Chevbot [3]. Another challenge with light power of a robot is the small amount of power which is actually usable by a solar cell due to efficiency of devices at the target size. To achieve desired power levels, several cells are often needed and must be connected in series which increases the size of the device footprint. This can be overcome to an extent by using photovoltaic tailored to a specific wavelength of light such as the infrared range, ultraviolet, or any color from the visible

spectrum. When tailored to a specific wavelength of light, these cells have much greater power efficiency than a solar cell with the same surface area.

2.3 Earlier Crawler Designs

Before showing the current design of SolarPede, we look at the previous designs of micro-crawlers which have led to its development of SolarPede. The Next Generation Systems micro-crawler has changed several times. Within this section is a discussion of the earlier designs in only as much detail as is necessary to explain the system. For further reading on each of the earlier designs, review the references used in the subsections of this chapter which are fully laid out in the REFERENCES section at the end of the document.

2.3.1 Previous Electronic Backpack Designs

In this section is a full presentatoin of the various printed circuit boards which have been used to test, drive, and improve the various Next Generation Systems micro crawlers. The previous boards include a variety of micro controllers, control strategies, and components. Each of these components was considered when designing the current version of SolarPede. After the description of all boards, there will be a table categorizing the things taken or learned from a particular desgin.

2.3.1.1 ARRIPede Version 1

The ARRIPede [35] was an untethered, micro-assembled MEMS microrobot, capable of stick-and-slip operation while powered by an on-board Lithium-Polymer battery similar to the LP30 FR Bahoma [35]. It featured a DSPIC33F Microcontroller

from MicroChip and several unnamed components such as a Voltage Regulator, Current Regulator, and Switch Mode Power Supply. For the purposes of this document, this micro crawler will be called the ARRIPede Version 1 (V1). The ARRIPede V1 can be seen below in Fig. 1.

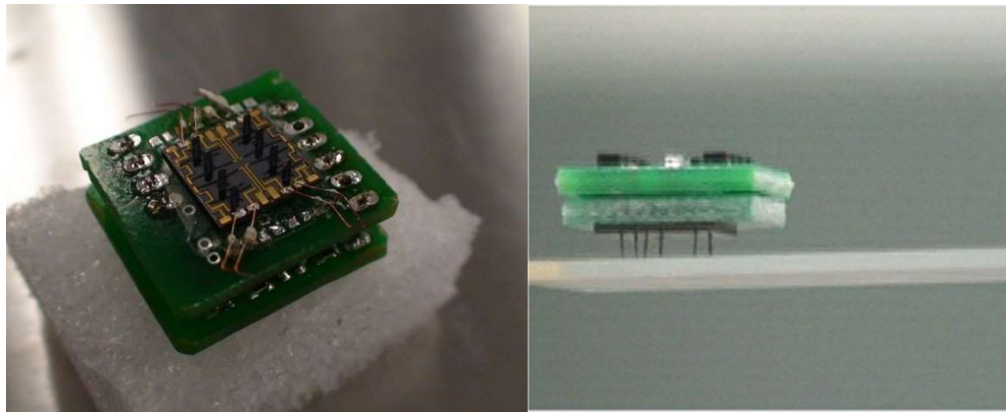


Figure 1. Shows the ARRIPede V1. Left) Assembled Prototype in “belly up” position. Right) Assembled Prototype in “belly down” position [35].

The ARRIPede’s gait and locomotion methods have been well characterized in past work and accompanied by stick-and-slip dynamical models [36]. This early design demonstrated a great payload carrying capacity in excess of 5g, and non-holonomic mobility characterized by forward only and large turn radii with speeds more than 1mm/s. However, the operation of this microrobot was seriously limited due to a short battery life (approximately 10 minutes), a nonholonomic motion dexterity on the substrate, and the lack of wireless communication for start, stop and feedback control.

2.3.1.2 Capstone 2017, ARRIPede Version 2

In 2017, more than 8 years after the realization of the original ARRIPede, a team of students from the University of Louisville endeavored to resurrect the ARRIPede

project. A senior design project which was sponsored by Dr. Dan O. Popa saw to the modernization of the ARRIPede V1 ideas [37]. The team redesigned the power electronics for the system and created what has since been called the Version 2 (V2) ARRIPede. The layout was implemented on a large board, approximately 4" x 2", intended for the testing of components before miniaturization to a size of 15mm x 15mm. New components include a TPS55340 [38] voltage booster from Texas Instruments, a transistor array made up of DMN63D8LV dual channel MOSFETs from Diodes Inc., and bluetooth compatible microcontroller, the CC2640 from Texas Instruments. The board can be seen below in Fig. 2.



Figure 2. Shows ARRIPede V2. Left) Pads only. Right) Fully Assembled [39].

Although this design would serve as the basis for nearly every design to follow, the board was not perfect. Despite its purpose, the methods with which these components would be tested were clearly an after thought. For example, the pins near the transistor array are not of standard spacing. This makes soldering of test pins difficult and prone to failure. Additionally, only one of the I/O pins on the microcontroller was connected to a test pin. To subvert this issue, one could probe the pins of the transistors directly, but due

to the small size of the DMN63D8LV, a typical probe is too large and touches multiple pads which shorts and destroys a transistor upon probing.

The strength of this design is in its component selection as all of the components used in this board have smaller counterparts. The microcontroller in particular was 7mm x 7mm as implemented on the V2, but has a ball grid array version which is only 3mm x 3mm. The CC2640 Microcontroller was among the latest from Texas Instruments at the time, and the voltage booster worked exactly as intended with output within 1.5% of the target. The transistor itself was also correctly chosen to meet design requirements, but the dual package of that transistor was too small for testing. Despite its flaws, this V2 was directly used for the design of the Version 3 ARRIPede below and its Voltage booster was used in several SolarPede experiments.

2.3.1.3 Capstone 2018, ARRIPede Version 3

The Version 3 (V3) ARRIPede was a direct continuation of the project started in Fall 2017 [39]. In Spring 2018, another team of students sponsored through the same project under Dr. Popa sought to follow through with the miniaturization of the V2 ARRIPede. The team also attempted to test the ARRIPede V2 and write a program for the micro controller. The V3 was expanded to feature 2 boards called the Top Board and Bottom Board. These were to be connected using a mezzanine connector [40] which was not included in the V2 and was among the only components new to this design. The V3 Boards can be seen in Fig. 3 and Fig. 4.

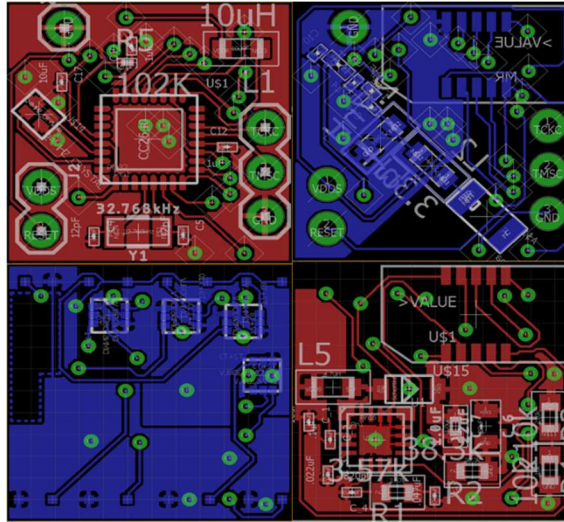


Figure 3. Shows the Eagle Layout of the ARRIPede V2. Top Left) Shows the top face of the Top Board. Top Right) Shows the bottom face of the Bottom Board. Bottom Right) Shows the top face of the Bottom Board. Bottom Left) Shows the bottom face of the Bottom Board [39].

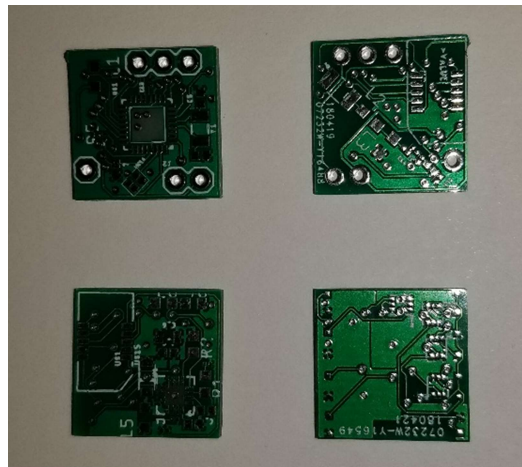


Figure 4. Shows the Printed Boards for the ARRIPede V2. Top Left) Shows the top face of the Top Board. Top Right) Shows the bottom face of the Bottom Board. Bottom Left) Shows the top face of the Bottom Board. Bottom Right) Shows the bottom face of the Bottom Board [39].

This new board faced many of the same challenges introduced by the V2 which were discussed above. Because testing the V2 was very slow, the design of the V3 was also slow. This meant that the team did not have time to assemble the new board before the project's end. Additionally, the programming of the CC2640 without a development kit is quite difficult. Texas Instrument's TI-RTOS is a language with a steep learning curve and a complex coding environment. Because the CC2640 was so new at the time of this board's construction, support for this particular controller was limited. Texas Instrument's main tech support resource is a living forum in which employees and customers alike share knowledge and skills to solve problems and challenges. Due to the relatively recent release of the controller, the information on issues was limited as few had used the newest controller.

Despite the untested nature of the V3, it gave way to the implementation of the micro crawler design across 2 boards. Additionally, it provided much needed PCB design practice and skills necessary to create future boards. It also introduced the Mezzanine connector used in the SolarPede V1.

2.3.1.4 Independent Study 2018, SolarPede Version 0

An independent study was conducted following the designs of the V2 and V3 boards. During this study, a new PCB was designed to use the same control strategies and methods of the previous boards. Like the V3, this board features a voltage booster, microcontroller, and transistor array. However, it did not feature 2 boards, but instead had 1 board which was of equal size to the microcontroller module with which it was paired. This new controller RFD22301 by RF Digital was part of the RFduino series of

controllers. RF Digital specialized in small scale microcontroller modules which were stackable and compatible with Arduino. Because the TI-CC2640 was so difficult to program without experience, the new design was geared toward known methods. The RFD22301 would be stacked and effectively take the place of the top board. Castellated edges were added along the bottom board to be bound to the RFduino. The resulting EagleCAD® design can be seen alongside the RFduino below in Fig. 5.

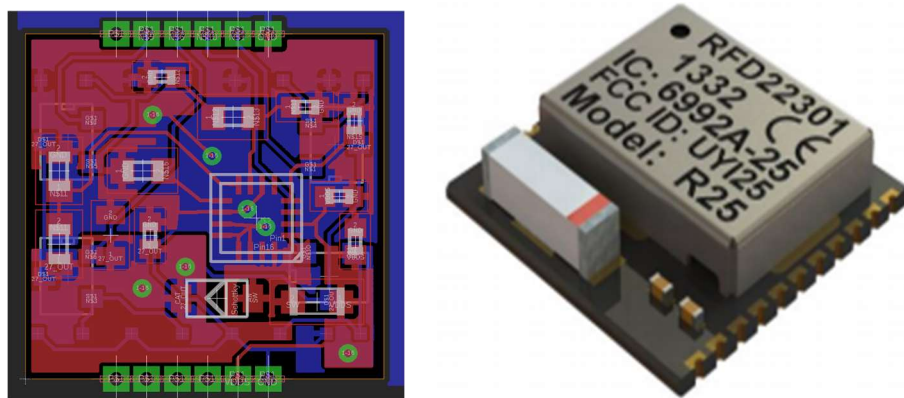


Figure 5. Shows the SolarPede V0. Left) Power Systems Board with castellated through hole connections. Right) RF Digital RFD22301 controller with antenna.

The SolarPede V0 includes all features desirable for the operation of the robot. A small, light weight, and wireless module with a footprint under 15mm x 15mm. Unfortunately, RF Digital was purchased by another company in 2015. In the summer of 2018, mere weeks after the completion of the SolarPede V0, the support for the RF Digital software was removed by its parent company. The libraries and .json files which are needed for the operation of the microcontroller were redacted, making the modules useless. Because of this discontinuation, a new redesign was required. The design which follows this one is the current SolarPede, and it draws heavily on this design despite the fact that the V0 was never implemented.

2.3.2 Previous MEMS Layouts

The ARRIPede V1 was tested and verified in [36] using the body shown in the left Fig. 6. Within [36] are two additional designs for MEMS bodies for future ARRIPede generations. The first is the ARRIPede belly type 1 shown in the middle of Fig. 6. This theoretical design was intended to provide omnidirectional movement to the ARRIPede. The second design is the ARRIPede belly type 2 which is shown in the right of Fig. 6. This design features legs facing opposite directions with the hope that the legs would provide a desired backward motion not available to the ARRIPede V1, but its functionality was never verified. Due to its similarity to the original body, it is unlikely that it would perform much differently.

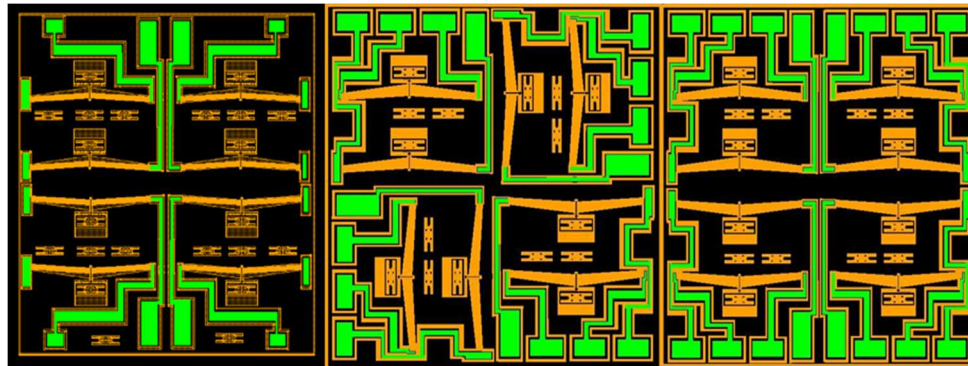


Figure 6. Shows ARRIPede V1 MEMS layouts generated using LASI. Left) Shows ARRIPede V1 Belly. Middle) Shows type 1 belly with theoretical omnidirectional movement. Right) Shows type 2 belly intended to add backward movement [36].

The ARRIPede V2, V3, and SolarPede V0 were designed to be connected to the layout shown in Fig. 7. That layout is a slightly modified Type 2 ARRIPede Belly shown in the right of Fig 6. It is virtually the same as the one shown in Fig. 6, but with some thickness changes to the beams and legs.

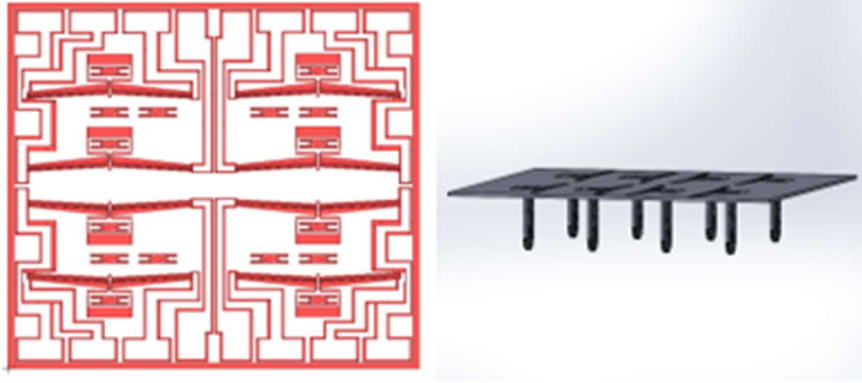


Figure 7. SolarPede L-Edit mask #1 (ARRIPede) and CAD model [41].

CHAPTER 3

DESIGN AND MODELLING

3.1 SolarPede Current Design

The SolarPede V1 (just called SolarPede from this point forward) micro crawler is a combination of the best elements of the previous generations of micro crawlers. In addition to combining the positives of the robots which came before it, the new SolarPede also features a completely redesigned leg layout which allows for omnidirectional movement.

3.1.1 Current Electronic Backpack design

The current electronic backpack includes many of the components from the earlier designs in section 2.3. The table below shows which of the components, features, or items from the older generations of electronic backpacks will be included. It also attributes the appropriate design with the introduction of the concepts. Below Table 5. is Fig. 8, a general system diagram. This diagram shows the basic formula with which the design was made and shows the roles that each component is intended to fill.

Table 1.

Shows the items duplicated on the current SolarPede design and gives reasoning as to why the respective component is to be included.

<i>Board</i>	<i>Item(s)</i>	<i>Reasoning for Inclusion</i>
ARRIPede V1	2 Board Design	Board components are dated, but the general design is very sound.
ARRIPede V2	TPS55340 Booster	Perfect for design requirements and specifications
ARRIPede V3	Mezzanine Connector	Simple way to compact many signals into a small area and transition between boards.
SolarPede V1	Transistor Array	Improvement upon V2 transistors, easier to test and better performance for high voltage.

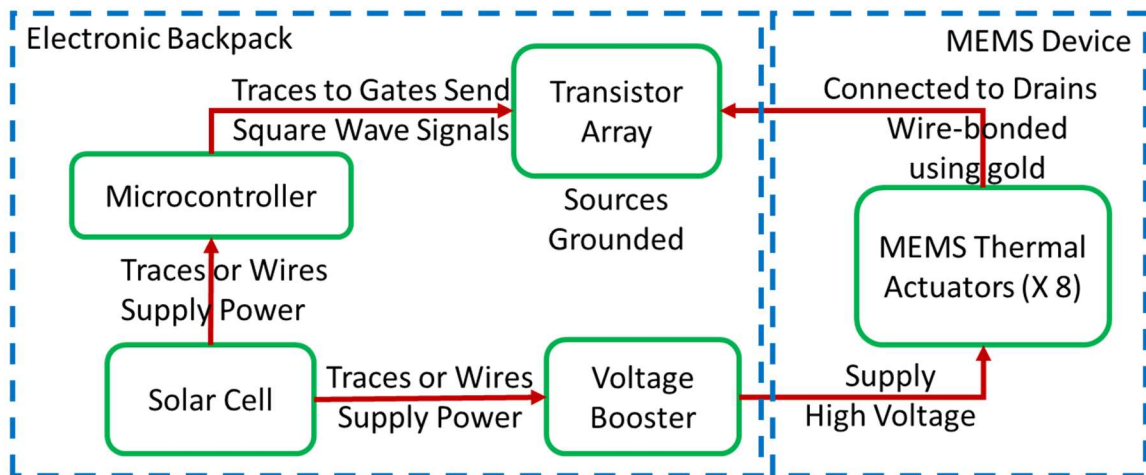


Figure 8. SolarPede system diagram. Rounded rectangles indicate a component used in the micro crawler. The arrows show some shared or provided resource and the delivery method. The blue dashed rectangles show on what the component will be mounted.

The current generation of printed circuit boards draw heavily on the ARRIPede V3. Although the layout for the Bottom Board is completely different and new, the schematic is virtually unchanged from the V2. The only major difference in the schematic is that the transistors used are a bit larger for easier probing and assembly. The Top Board is completely changed. Because the CC2640 is quite difficult to program, a new controller is used.

3.1.1.1 Die Testing Board

In response to the challenges faced when experimenting with the V2 board, a testing board was made for the SolarPede V2 design. This board is two parts joined by through hole pins. The first board features an array of pads arranged to be easily wire-bonded to a MEMS die. This board (called the Die Board) is small and easily replaceable. The second board (called the Base Board) houses the transistors and microcontroller. This board can be connected to using UART and power can be supplied using either a power supply or the voltage booster. This board is shown below in Fig 18.

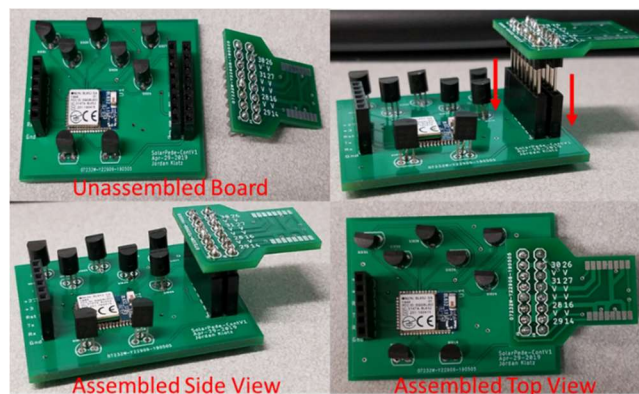


Figure 9. Shows the Die Testing Board for SolarPede V2. It shows the process of attaching of the Die Board to the Base Board from several angles.

The new SolarPede is implemented over 2 boards, features a BL652 from Laird, TPS55340 Booster from Texas Instruments, and Transistor Array made of DMN63D8LVs from Diodes Incorporated (These transistors were originally considered for the V2 board, but not utilized to save space). The two boards will be joined by a mezzanine connector like the one selected for the V3 board.

3.1.2 Current MEMS Layout

Compared with ARRIPede microrobot shown in Fig. 6, which has nonholonomic locomotion [36], new leg arrangements were configured to explore omnidirectional motions corresponding to the layout in Fig. 10, the SolarPede omnidirectional design. The inspiration of the placement of legs in these designs comes from similar Mecanum wheels or differential drive arrangements for larger modern mobile robots. These legs were arranged to create motion as in Fig 11. and Fig 12.

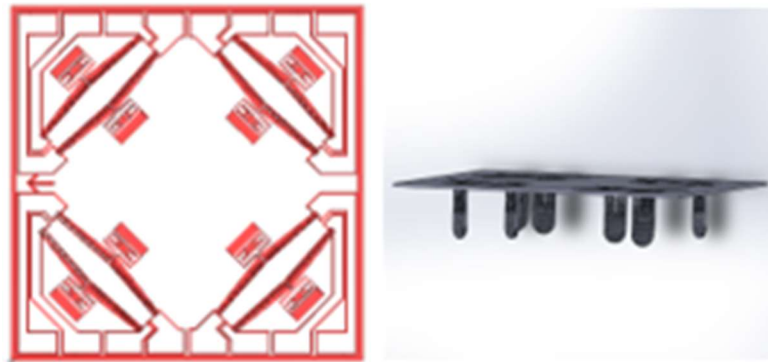


Figure 10. SolarPede L-Edit mask #2 (omni-directional) and CAD model [41].

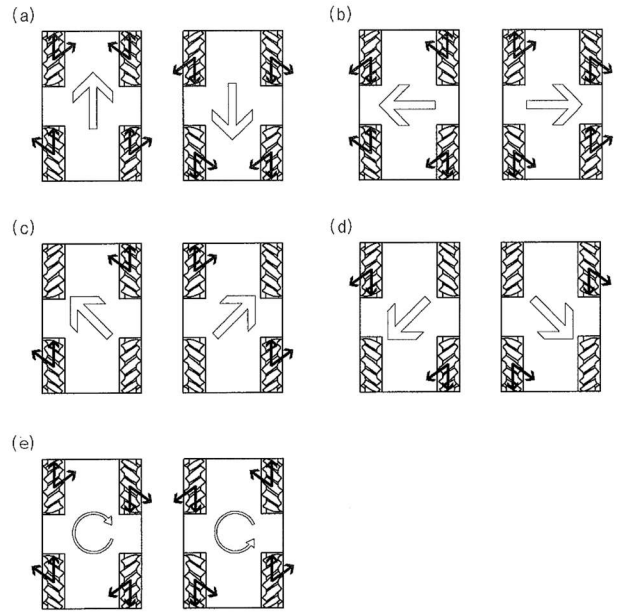


Figure 11. Shows mecanum style wheels with vectors of motion for individual wheels to generate body motion in the direction of the large arrow.

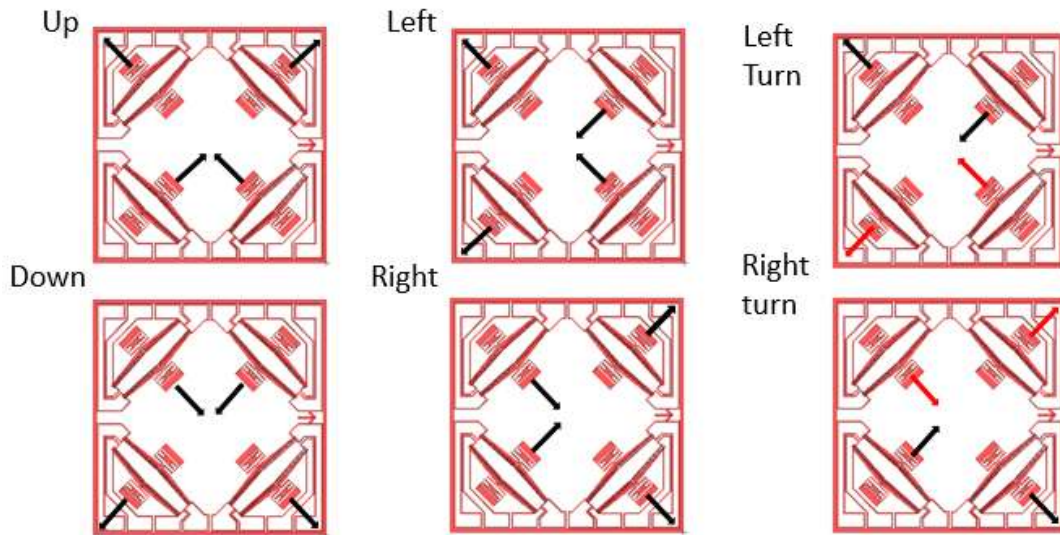


Figure 12. Shows current SolarPede body layout with vectors theorized for the replication of the mecanum behavior as shown in Fig. 11. Black arrows indicate a typical actuation of a high frequency while red arrows indicate a lower frequency. A difference in speed

between the left or right sides should result in the rotation of the robot in a particular direction.

3.2 Modelling

The movement of SolarPede is caused by the heating and cooling of the chevron beam legs. When heating, the beams expand causing a forward motion of an individual leg. During cooling, leg instead pulls the robot forward slightly. Over repeated actuations, the net result is forward motion. This is possible because of the friction between the top of the leg and the body as well as the friction between the bottom of the leg (foot) and the ground or a payload. In figure 7 is the free body diagram of a single leg for SolarPede which was used in a lumped thermo-mechanical model.

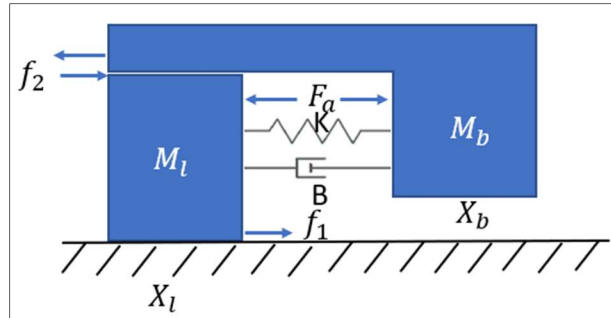


Figure 13. Mass-spring-damper free body diagram for SolarPede [41].

In the figure, f_1 represents the friction between the foot and surface while f_2 represents the friction between the top of the leg and the body. M_l is the mass of the leg, approximately $.3mg$, and M_b represents the mass of the body, approximately $.25g$. F_a is the force introduced through the applied voltage V , and opposed by both K , the spring constant, and B , the damping coefficient (chosen to be $.1$). This expansion results in

displacements X_l and X_b which are the displacements of the leg and body respectively.

These were used to generate the equations below.

$$M_l \ddot{X}_l = -F_a + f_1 + f_2 + K(X_b - X_l) + B(\dot{X}_b - \dot{X}_l) \quad (1)$$

$$M_b \ddot{X}_b = F_a - f_2 - K(X_b - X_l) - B(\dot{X}_b - \dot{X}_l) \quad (2)$$

$$f_1 = \mu(M_b + M_l)g \quad (3)$$

$$f_2 = \mu M_b g \quad (4)$$

In the equations above, μ is either static ($\mu_s = .4$) and dynamic friction ($\mu_d = .33$) depending on whether the robot leg is sticking or slipping. F_a is the force introduced on the system by the heating of the beams estimated using Eq. (5) which represents the thermal portion of the model. This thermal actuation is like a disturbance on the mass-spring-damper system.

$$F_a(V, f) = \frac{2NAE \sin^2(\theta)}{L} \cdot \frac{\lambda V^2}{1 + s \frac{f}{f_{BW}}} \quad (5)$$

N is determined by the number of chevron beams (6 in this case), and A is the cross-sectional area of those beams ($W = 1 \mu\text{m}$, $L = 1 \mu\text{m}$). E is the Young's modulus of silicon which is 165 GPa. The angle θ is the angle of the chevron beams which is 3.4° for SolarPede. The actuator frequency and bandwidth are f and f_{BW} respectively. To verify this lumped model, a solid works model was generated and tested using MATLAB. The results were used to obtain constants and terms needed for the full model. The final lumped model was realized in MATLAB (See APPENDIX C for code created by Zhong Yang, a fellow researcher in the lab) then tested using frequencies and applied voltages as discussed in Experimental Setup 5.1.

CHAPTER 4

FABRICATION AND PART SELECTION

4.1 Part Selection

Powering and control systems for the SolarPede are housed within the electronic backpack. This section details the choices of components utilizing the information from Section 3.1. The components were selected to fill the roles portrayed in the system diagram in Fig. 14. At the end of the section, is a new system diagram with the chosen components.

4.1.1 Voltage Booster

To move the Chevron actuators on the microrobot body, a minimum voltage of approximately +8V is required; however, to obtain sizable, micron-scale displacements, voltages in excess of 20 V are needed. A voltage booster and supporting components are placed on one side of a printed circuit board, and converts +3.3 V applied at power source input which will produce an output of at least +20 V. This general target output value was chosen based on tests for the thermal chevron actuators used in our previous work with microrobots ARRIPede [39] and sAFAM [4]. The SolarPede utilizes a TPS55340 Booster, Texas Instruments, USA due to its output characteristics and low power input requirements [38]. The following equation from the voltage booster data sheet can then be used:

$$V_0 = 1.229 * \left(\frac{R_1}{R_2} + 1\right) * V_i \quad (6)$$

in which R_1 and R_2 are tunable resistors. To fulfill system requirements, these values are chosen to be 160k and 10k respectively which results in an output voltage of 20.9 V from an input voltage of 3.3 V.

4.1.2 Transistor Array

The transistor array serves the purpose of regulating current to the Chevron actuators and stopping the flow of current to the legs when actuation is not desired. The drain of an N-Channel MOSFETs will be connected individually to the second pin of the thermal actuators. When an input of 1.8 V or greater is applied to the gate of the transistor, the circuit will be complete, and actuation occurs. The boosted voltage will be applied to one pin on of the 8 actuators in the MEMS system. Transistors will be placed in series with the actuators and be used to control which actuator is heated.

The array itself will consist of 8 DMN62D0U (Diodes Inc., Plano, Texas, USA) transistors all of which will be mounted to the bottom of the electronic backpack, near the legs for easy access during wire-bonding [42]. These were chosen to accommodate the +3.3 V output of the microcontroller as well as the drain voltage of +20.9 V.

4.1.3 Micro Controller

A microcontroller is necessary to ensure that SolarPede is capable of untethered control. The microcontroller will represent the control system of the SolarPede and will be responsible for communication with the user and for the generation of signals which

actuate the various legs of SolarPede. It will be connected to both the solar cell and the transistor array on the Electronic backpack.

4.1.3.1 Communication Protocol

Several microcontrollers were considered for the design. The primary determining factor for the microcontroller was the communication method. A study was performed on the advantages and disadvantages of various communication methods available in microcontroller technologies. Wi-fi, ZigBee, Xbee, Bluetooth (and BLE) 4.0/4.2 and 5.0, Infrared, and Terahertz were evaluated on reliability, size of systems, range, data transfer speeds, power consumption, and existing applications on micro systems similar in scale to SolarPede [43-51].

Each of the methods were ranked against one another and given points based on placement in the ranking for each category (5 for 1st, 4 for 2nd, etc.), as summarized in Table 1. Rows show individual ratings in the evaluated categories. Range was measured in feet. Data Rate was measured in (k, M, G) bits/second. Reliability was evaluated through general review and feedback from the academic community. Size was evaluated by comparing typical module footprint for systems used in micro robotics applications. Power Consumption was measured in W (or mW). The Existing Micro Robot category was a simple count of published journal and conference papers with robots of similar scale to SolarPede. The final column, Total, shows total points accrued during comparison.

Table 2.

Communication method points for rankings in comparison study [41], [43-51].

	<i>Range</i>	<i>Data Rate</i>	<i>Reliability</i>	<i>Size</i>	<i>Power Cons.</i>	<i>Existing Micro Robots</i>	<i>Total</i>
<i>Wi-fi</i>	4	5	5	1	1	3	19
<i>Infrared</i>	1	4	4	4	2	5	20
<i>TeraHertz</i>	2	3	1	5	5	1	17
<i>Bluetooth 4.2</i>	3	1	2	2	3	4	15
<i>Bluetooth 5.0</i>	5	2	3	3	4	2	19

Two things should be noted before continuing. Firstly, Xbee and ZigBee were both studied as stated above, but since they received the lowest markings in all categories, they were not included in the table. Secondly, while the table also implies that Bluetooth 4.2 is of poor quality, it should be viewed as having an equal ranking with Bluetooth 5.0 in several categories. Since no ties were permitted in the scoring, the table can be misleading. In the case of a tie between Bluetooth 4.0/4.2 and Bluetooth 5.0 (As with Data Rate, Reliability, Size, Power Cons.) it was determined that V 5.0 would receive the advantage as it is the newer technology. If the advantage was given to 4.0/4.2 on a tie, or if the two had received equal points, the table would present a more obvious correlation.

The resulting table (Given the notes) shows that Bluetooth 5.0, Wi-fi, and Infrared have strikingly similar performance. Because of the very close scores, a determination was made that certain categories were more important to the specific application of SolarPede. Size and Power Consumption were viewed as the most important, so Wi-fi was easily eliminated. Performance tradeoffs could still be argued between Bluetooth and

Infrared, but because SolarPede is to be powered by light, it was decided that Bluetooth should be used over infrared to avoid possible interference from incoming light.

4.1.3 Micro Controller Cont.

Taking all findings into consideration, a logical starting point for the controller search is actually the SolarPede V0 design whose microcontroller was Bluetooth 4.2 enabled. The company which discontinued the original controller for the V0 is called the Laird Corporation, USA. Laird Connectivity, a branch of the greater corporation, specializing in Bluetooth and Wi-fi microcontrollers such as the BL652 [52] which are ideal for SolarPede's system requirements. This module was originally a Bluetooth 4.2 module, but it has been updated to Bluetooth 5.0. The BL652 is among the newest microcontrollers from Laird, and it features more than enough Special Input Outputs (SIO) to support SolarPede. These SIO are individually customizable to PWM, Digital I/O, Analog I/O, and Frequency modes which allows for a dynamic control of SolarPede if future designs utilize another control strategy. The BL652-SA module also includes an onboard antenna which sets it above some of the controllers from other manufacturers which would require an antenna to be included on the PCB, thus making the footprint larger. As manufactured, the module also only occupies a 10mm by 14mm footprint and is easily coupled with the electronic backpack.

4.1.4 Solar Cell

Among the primary concerns with the SolarPede designs is the goal of keeping the system completely untethered. To accomplish this, input power is provided directly to the voltage booster from a solar cell that allows the operation of the robot under an

artificial white light source. The solar cell in our prototypes, is a 3 V Solar Cell, Solar Made Corporation, Colorado, USA, and was selected to balance the power consumption of the micro-actuator, with the power generated on a limited 20 mm x 20 mm footprint.

4.2 Assembled Backpack

The complete system diagram for SolarPede is shown in the diagram in Fig. 14. As designed, the backpack can further be split into a power system and control system. The control system is the micro controller and transistor gates while the power system is the solar cell, the voltage booster, and the rest of the transistor array. The power system is used to supply the MEMS actuators directly while the control system regulates which actuators are connected to the power systems at a given moment. These work in conjunction to create the gait patterns required for steerable motion.

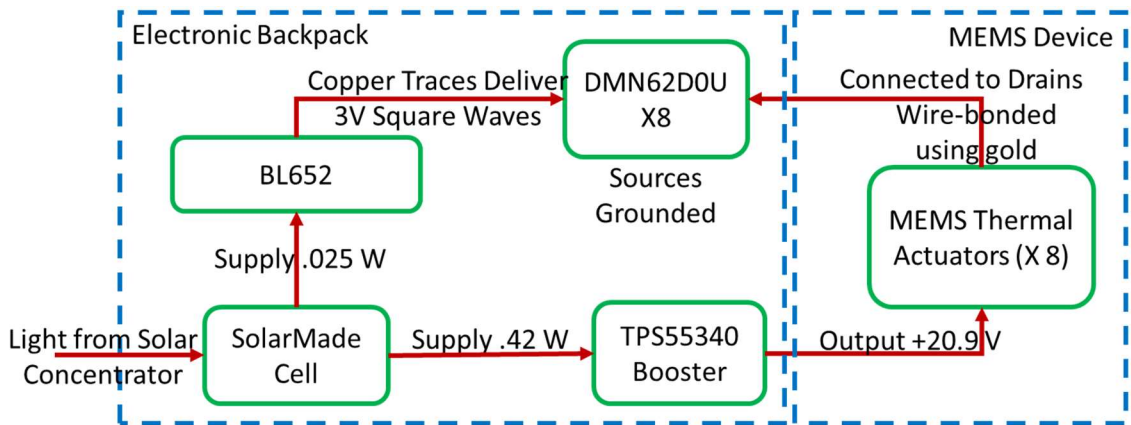


Figure 14. System Diagram showing components as chosen.

Utilizing the information gained during experimentation (discussed in CHAPTER 5), a final electronic backpack was realized. This backpack, which contains all components discussed in the part selection chapter, was assembled by hand and can be seen below in Fig. 15. The two boards were printed with different finishes. The top was

made using Hot Air Solder Levelling (HASL), a standard finish, and the bottom was made using an Electroless Nickel Immersion Gold (ENIG) finish serves the dual purpose of protecting the board from wear and tear and makes wirebonding easier due to the addition of gold. This backpack's components were tested to the best of our capabilities as discussed in the breadth of CHAPTER 5 and CHAPTER 6.



Figure 15. Shows the final electronic backpack assembled. The board on the left houses the microcontroller and necessary UART connections. The board on the right is the bottom board which contains power components including the voltage booster.

4.2 Body Fabrication and Packaging

The body and legs of SolarPede are fabricated on a silicon-on-insulator (SOI) wafer with following parameters: the device layer is 100 μm thick, $\langle 100 \rangle$ orientation, and N-type with 0.01 to 0.02 $\Omega\text{-cm}$ resistivity; the buried oxide layer is 2 μm thick; and the handle layer is 500 μm thickness and P-type with larger than 1000 $\Omega\text{-cm}$ resistivity. In Fig. 16 is a diagram showing the workflow of the SOI process.

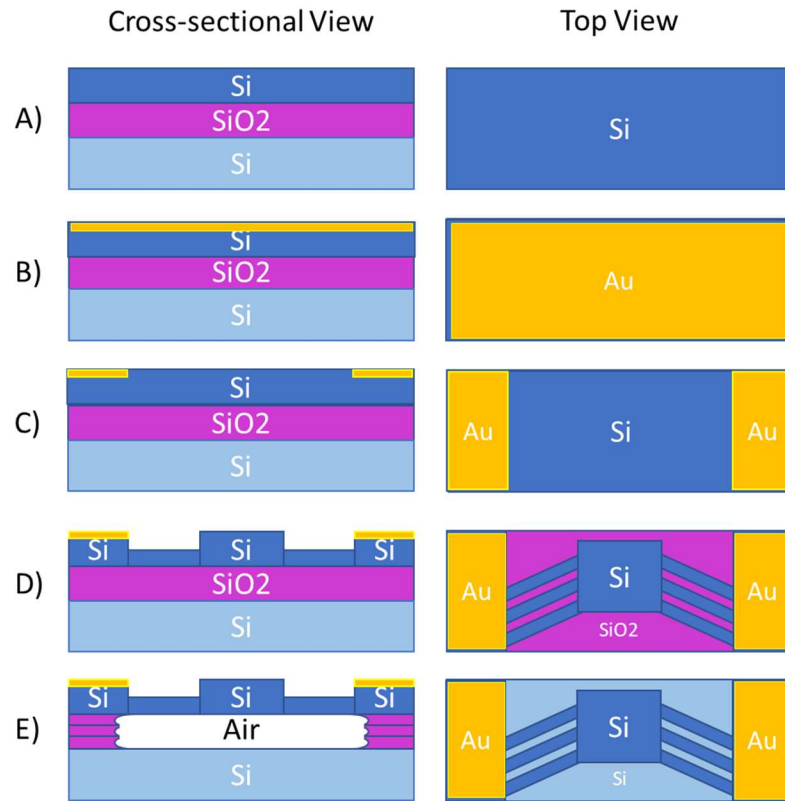


Figure 16. Top and Side views of a typical wafer during SOI fabrication of SolarPede. (SiO₂ width made larger for visual). A) Initial SOI wafer. B) Wafer after metal deposition. C) Metals patterned to define traces and contacts. D) Structure after DRIE process E) Final wafer after HF release.

An RCA clean of the SOI wafer is performed as the first step of fabrication, to remove any organic, oxide and ionic contaminations, followed by photolithography to define the MEMS actuator features. A thin layer of chromium is then sputtered with a PVD-75 sputter under DC mode with 300 W, to boost silicon-gold adhesion. A thick layer of gold for bonding points to the die package was sputtered under the same settings with longer sputtering time. Later, the metal is patterned with photolithography and then etched by gold etch and chromium etch consecutively.

A second photolithography is performed in preparation to for deep reactive ion etching (DRIE). To protect the wafer, a thick photoresist is deposited onto the wafer. Before DRIE, a full inspection is performed to cover all gold remnants after the patterning step. The etching time is derived from experience with the tool and conditions during the day of fabrication. Once etched, the wafer checked under microscope to confirm finishing of etching. Before dicing the wafer, a protective layer of photoresist was spun to prevent debris from damaging or jamming the moving features. After dicing, selected dies were submerged in 49% hydro-fluoric acid to release moving parts from the wafer surface. Eventually, all released dies were dried by critical point dryer (CPD) to finish the fabrication process.

4.3 MEMS Assembly

After the wafer is fabricated, the legs of SolarPede are assembled using a custom assembly station called the NeXus Micro Assembly Station or NeXus for short. The system can be seen in Fig. 17. The station is equipped with a motorized linear and rotational microgripper called M1, a 6 degree of freedom XYZ and θ stage and an extra manual XY stage which is called M2. M1 and M2 are responsible for manipulating and positioning the samples while under the watch of 3 different vision systems. The processed Die which will constitute the body of SolarPede is loaded onto M2. M1 is used to pick up unattached legs using a so-called jammer. These legs are then rotated to the appropriate angle and inserted into the aforementioned Zyvex Sockets. Once in position, the legs are adhered to the greater structure using epoxy which is hardens under exposure to UV light. Once glued in this way, the legs become reinforced and strong enough to

support the weight of a payload or the SolarPede itself. In Fig. 18 is a model of a single leg generated using Solid Works. To the right, in the same image, is a picture captured using the NeXus imaging cameras.

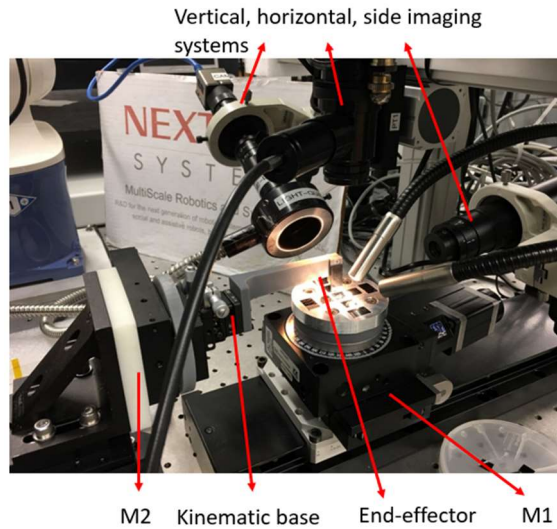


Figure 17. NeXus Micro-Assembly System M1) Manipulator with vacuum tipped microgripper on X-Y- θ motorized stage. M2) 6 DOF positioner stage consisting of motorized X-Y-Z- θ and manual X-Y [41].

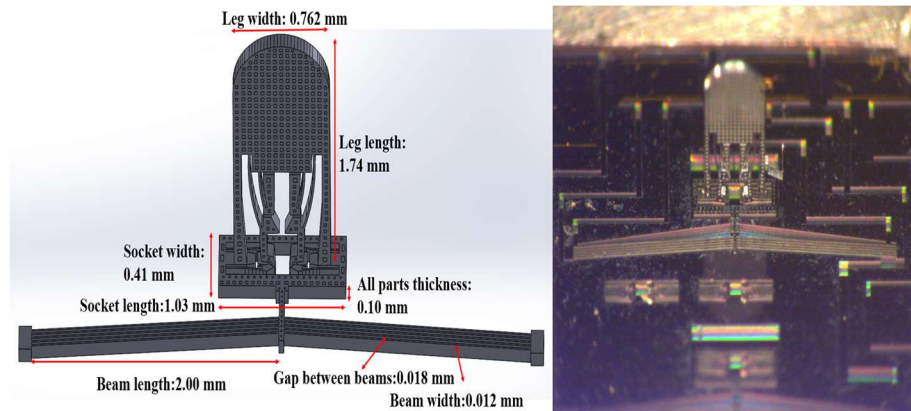


Figure 18. SolarPede legs assembled. Left) SolidWorks model of leg with dimensions recorded in Table 1. Right) Actual assembled leg imaged while in M2 of NeXus station [41].

Table 3.

Dimensions for items shown in Figure 18 left.

<i>Item</i>	<i>Measured Value</i>	<i>Item</i>	<i>Measured Value</i>
Leg Length	1.74 mm	Beam Length	2 mm
Leg Width	0.762 mm	Beam Width	12 μm
Socket Length	1.03 mm	Beam Gap	18 μm
Socket Width	0.41 mm	Part Thickness	0.1 mm
Chevron Angle	3.4 degrees	Beam Count (N)	6

CHAPTER 5

EXPERIMENTATION AND VALIDATION

5.1 Set up and Tools

In this section is a full explanation of the setups and technologies used for 3 different categories of experiments. The three sections are Leg Displacements, Power Components, and Solar Cell. The leg displacement section is further divided into single leg, multi leg tests, and payload. In the multi-leg section is also a discussion of the control strategies which are used in subsequent experiments.

5.1.1 Set up for Leg Displacement Experiments

To build the behavioral model for SolarPede, tests were performed on a single leg. These experiments were used to collect data on the steady state, displacement, and rise time of the leg. Multi leg tests were also used to help generate the actuation patterns to be used in the different types of motion shown in Section 3.2.

5.1.1.1 Set up for Single Leg Experiments

The assembled legs must be validated to ensure the concept of SolarPede is sound. To do this, the die is packaged which is wired onto a breadboard. The bread board and package are placed in line with a laser displacement sensor (LK-H008 sensor head

with a LK-G5001 controller, Keyence Corporation, U.S.). This sensor measures the movement of the leg during operation. A power supply was connected through the bread board to the in-line leg and various voltages were applied the leg. The system was given ample time (30-40 seconds) to full extend while the sensor was used to measure corresponding displacement. The packaged die can be seen on a breadboard in Fig. 19.

This single leg set up was also used to check the switching speed of the leg. The leg was subjected to a square wave of varied amplitudes and frequencies with the displacement measured using the same sensor as before. Frequencies of 10 Hz, 20 Hz, 50 Hz, 100Hz, and 200 Hz were used. The average displacement and standard deviation for the combinations of voltages and frequencies are shown in Table 2 in the results section.

Lastly, this setup was used to generate a pseudo random binary sequence (PRBS). A square wave of varied frequency and duty cycle was applied to the leg and the displacement was measured. This PRBS was used in system identification and combined with the Ansys model discussed in section 3.3.

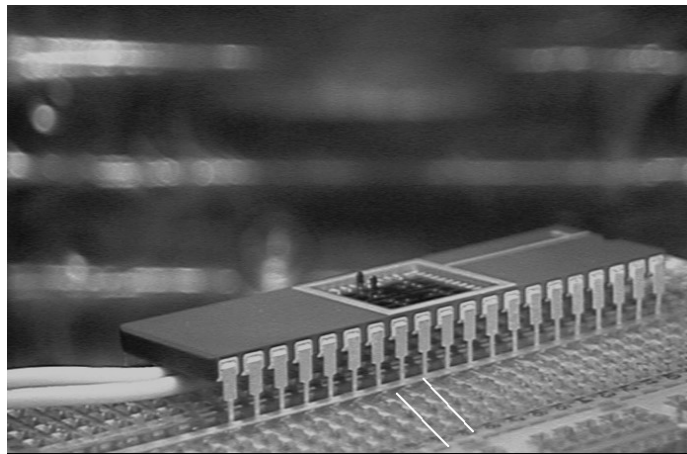


Figure 19. Single leg testing structure on bread board. Keyence sensor placed in line with this leg for measurement.

5.1.1.2 Multi Leg and Control Strategy

The Laird BL652 module can be interfaced through UART, SPI, I2C, VSP, and JTAG connections and is programmed using a custom language called *smartBASIC*. Programs are written in the programmer's editor of choice and compiled using a terminal program [53] [54].

The program for SolarPede begins by broadcasting the BL652's address to a Bluetooth compatible phone or computer. Once connected using the Laird app or terminal, a virtual serial port is opened. The user can then type into the serial port and transmit a string of characters to SolarPede. A simple case switch interprets the user input and performs a routine based on the user's selection. The routines activate the SIO (set to digital outputs) to digital high or low in a pattern. The patterns are "forward", "backward", "tleft", "tright", and "idle". The user can also select "complete" to stop the program and "testing" to activate only one leg. This testing allows a user to check the status of an actuator or transistor to ensure it is working. As a final feature, each time a user is prompted to select a gait option, he or she can also select a delay associated with the square wave to set the speed.

For the experiments, a voltage of +20 Volts is applied to the drain of transistors on the SolarPede circuit. The BL652 special input/outputs (SIO) are used to generate square waves with an amplitude of 0 or 3.3 volts. These signals are tied to the gates of the transistors such that when the output is high, the transistor is closed, and current can pass to the corresponding micro-actuator.

For the multiple leg experiment, the fully assembled die was placed under camera in “belly up” position. That is, the legs were facing up toward the camera and the package was beneath. The same power supply used in the single leg test was connected to the legs, but an NPN transistor was added in series with each leg. The gates of these transistors were connected to a micro controller which acts a multiplexor for the setup. Different patterns were tested to determine the behavior of the legs and the speed at which they would actuate in sequence. Below is Fig. 20 which shows an image of the assembled legs in the NeXus System as well as an image of the system under camera while bread boarded.

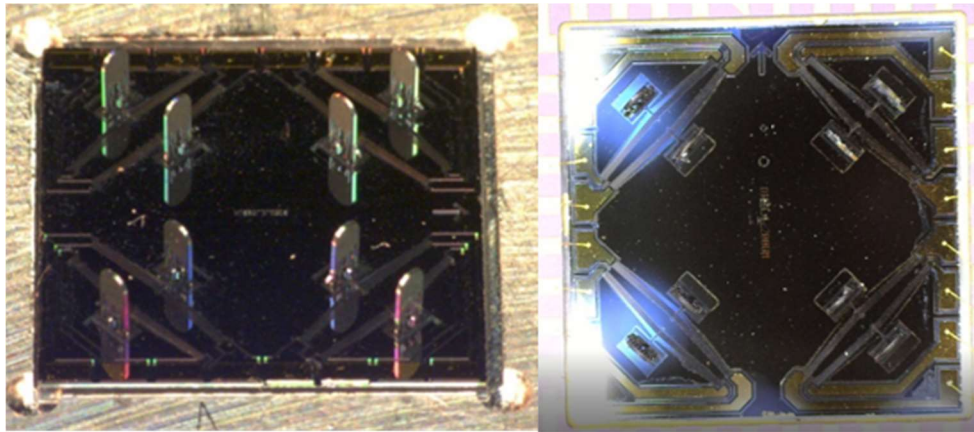


Figure 20. Left) Assembled Legs under NeXus Imaging System [41]. Right) Legs under camera during “Belly-Up” operation.

5.1.1.3 Setup for Payload Experiments

To simulate the operation of the assembled SolarPede, the circuit used during program and component validation was wired to the die carrier. The SolarPede legs were breadboarded and connected to a power supply. The legs were placed in series with

transistors which were connected to the SIO of the BL652. A payload cut from a silicon wafer was placed directly onto the legs of SolarPede, and the legs were actuated as described below to create motion of the payload. Placing a payload on the legs in this manner simulates the upright actuation of the robot under its own weight. This setup is similar to a micro conveyor like the one shown in [55] which also uses chevron thermal actuators. The motion of this payload was recorded with a microscope camera and the resulting footage was used to determine velocity of the robot.

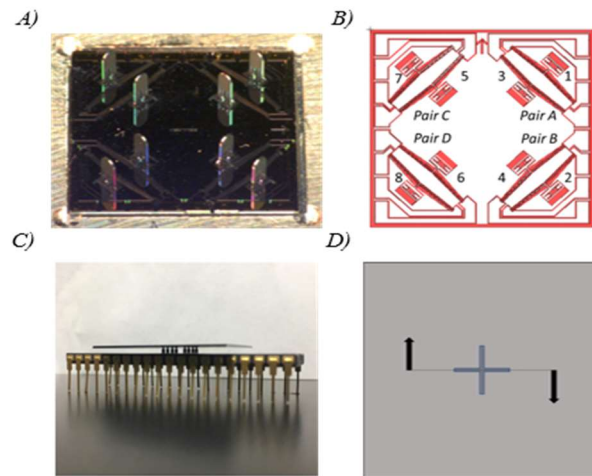


Figure 21. A: Assembled SolarPede Legs [41]; B: Legs labeled as in program with pairs marked [41]; C: MEMS die wire bonded and in a package with payload resting on top [41]; D: Vectors for payload motion under rotation gait sequence [41].

To protect the integrity of the equipment, light payloads were used initially. The die carrier was placed into the breadboard as before and the motion of 0.5, 0.6, and 1.2-gram payloads were recorded using a camera. The payload can be seen in Fig. 21 C and D. A cross shaped scratch was made on the surface of the silicon payload to make tracking the payload easy to monitor and the result is shown in Fig. 21 D. The payloads

were tested in succession having their motion recorded before switching to the next payload increasingly heavy.

5.1.2 Set up for validation of Light Power

The main goal of the SolarPede design is to make it possible to power the robot using light. To harvest this light, a solar cell will need to be used. The main restriction of the solar cell used is the footprint which needs to be around 20mm x 20mm. For our experiments, we utilized a SolarMade cell of 20 x 24 mm. Two experiments were conducted using this solar cell.

5.1.2.1 Power Output Validation

We placed the cell under a solar simulator from Newport Corporation, Irvine, USA, including a Xenon arching lamp (Newport 67005). From there, we exposed the cell to white light of increasing intensity and recorded the power output. Matching this to the input power to displacement chart makes it clear whether this solar simulator and solar cell are valid for the operation of the robot. Below in the left of Fig. 22 is the solar simulator aligned with the solar cell while it is connected to the SolarPede Die. On the right is a closer image of the simulator and cell.

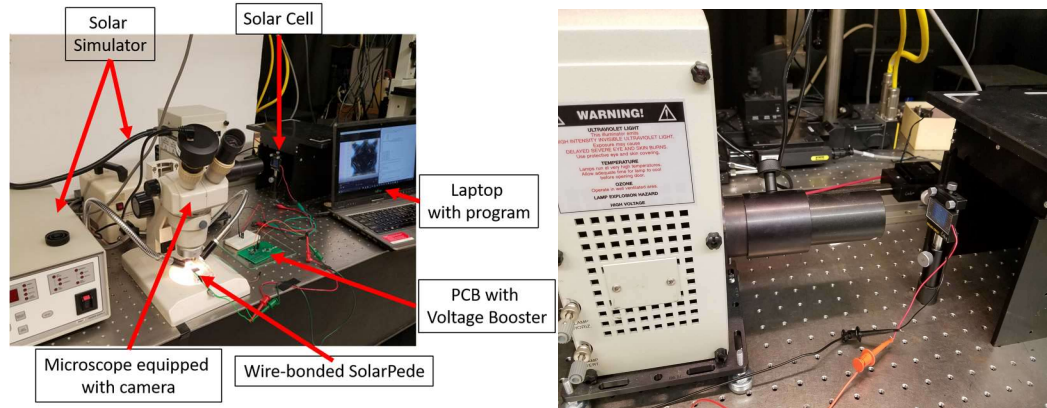


Figure 22. Solar cell and light power verification set up. Left) Set up with laptop and SolarPede [41]. Right) Close up of cell and solar simulator.

5.1.2.2 Light Power of The Electronic Backpack

The final experiment conducted during this research was to power the Electronic Backpack and demonstrate the actuation of a leg while being powered by light, a feat which would fully prove the design's validity. To realize this, the setup shown in Fig. 23, was used. With this setup, the Top Board from the SolarPede V1 backpack was used in conjunction with an FTDI chip for communication with the user PC. However, the bottom board has a flaw which prevents it from being utilized in this type of test, that is, it is designed for wire bonding directly to the SolarPede body and is not ideal for this experiment. Instead, the ARRIPede V2 board was used in conjunction with the top board (Also shown in Fig. 23). The two boards were placed in parallel with the Solar Cell and Powered. The displacement of the leg was measured using a camera with pixel counts representing the displacement in microns.

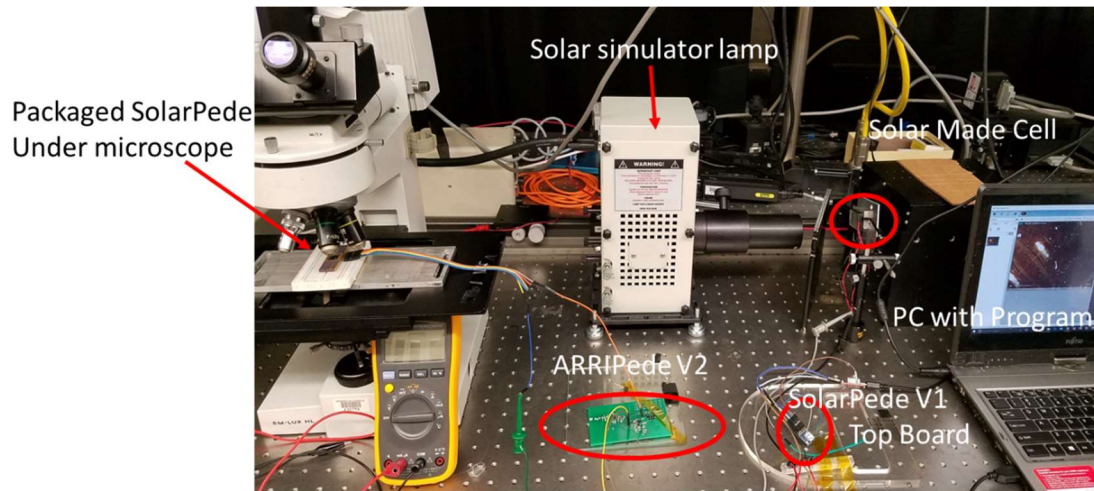


Figure 23. Shows the experimental setup for the powering of the SolarPede V1 electronic backpack using light emitted from a solar simulator lamp.

5.2 Experimental Results

Using the setups described in section 5.1, experiments were conducted to validate the motion and electronic backpack design. Experimental results are divided just as with section 5.1. Within each of the results sections are also any modifications to the system setup reported in section 5.1.

5.2.1 Leg Displacement Results

The experiments conducted with the legs verified the model and were used to generate gait patterns successfully. The specific results are discussed in conjunction with any shortcomings of the system.

5.2.1.1 Single Leg Experiment Results

Using the set up in 5.1.1.1 and the program generated in 5.1.1.2, experiments were conducted for the steady state model of SolarPede. The “testing” feature of the program was used to generate a signal only to a select leg. This leg was positioned in line

with the laser displacement sensor in 5.1.1 and was used to measure the displacement of the leg during operation. A voltage was applied to the leg and then the leg was given 30 seconds to fully extend. This is more than enough time for the leg to reach a steady state. Several different voltages were used for the experiment. Starting with 5 V's and increasing to 30 V, the displacement at these values were recorded. The input power was calculated based on the applied voltage and plotted against the displacement observed under the laser. Figure 24 presents the results and demonstrates a fairly linear relationship between power and displacement.

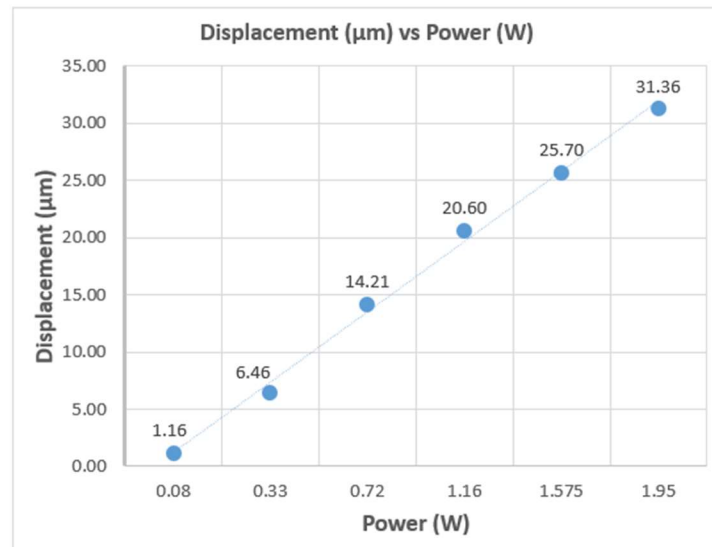


Figure 24. Shows the average displacement vs power for single leg experiments with legs given full time to extend [41].

Once the average displacement was measured in a steady environment, an experiment was performed to test the leg's behavior with varied voltage and frequencies. Leg displacement results from relevant combinations of voltages and frequencies can be seen in Table 2. Using the data collected, 60 samples were taken from wave forms and used to calculate the mean and standard deviation of the displacement. The nominal

operating range for the SolarPede was determined to be from 0 to 50 Hz. When larger frequencies, such as 200 Hz are applied, the actuators do not have enough time to cool. As a result, they will not retract from the steady-state displacement, and the leg remains extended and vibrates in that position.

Table 4.

Shows input voltage to the SolarPede leg, the frequency of 3.3 V amplitude square waves at the transistor gate, the typical maximum actuation in micrometers, and the standard deviation [41].

<i>MEMS actuator Voltage</i>	<i>Gait Frequency</i>	<i>Average displacement</i>	<i>Standard Deviation</i>
10V	10 Hz	2.96 μm	0.01 μm
10V	20 Hz	3.03 μm	0.02 μm
10V	50 Hz	2.34 μm	0.07 μm
10V	100 Hz	1.57 μm	0.14 μm
20V	10 Hz	12.42 μm	0.04 μm
20V	20 Hz	12.48 μm	0.03 μm
20V	50 Hz	9.89 μm	0.21 μm
20V	100 Hz	6.14 μm	0.50 μm
30V	10 Hz	25.20 μm	0.07 μm
30V	20 Hz	22.37 μm	0.02 μm
30V	50 Hz	17.81 μm	0.34 μm
30V	100 Hz	11.24 μm	0.96 μm

The results shown in Table 2 suggest that frequencies of 50 Hz may not be effective for actuation, because the leg does not reach a steady state in the short time that

the voltage is applied. Due to the short switching time, the leg displacement is much smaller than at lower frequencies.

The model and simulation in MATLAB were used to obtain $K = 185 \text{ N/m}$, $\lambda = .03$, $f_{BW} = 50 \text{ Hz}$. The model was used to generate the plots in Fig. 25 which predict the relationship between frequency, voltage, and velocity.

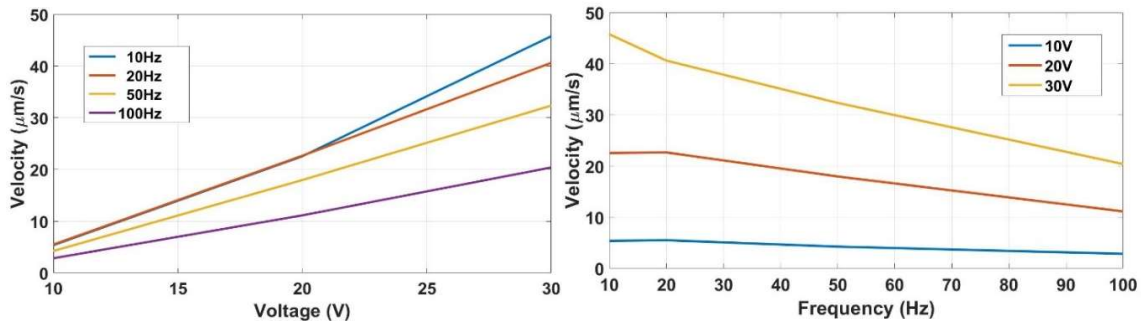


Figure 25. Left) Plot of robot body velocity vs applied voltage for a range of frequencies [41]. Right) Plot of robot body velocity vs applied frequency for a range of voltages [41].

The data obtained through experimentation suggests that if the model is accurate, velocities should be in excess of $10 \mu\text{m/s}$ for tested frequencies so long as the applied voltage is above 20 V. Additionally, velocity is shown to increase with supplied voltage but decrease with increase in frequency.

5.2.2.2 Multi Leg Test Results

The program utilized in the single leg experiments was modified for a test with multiple legs while still in “belly up” mode. This time, the signals were multiplexed to each of the 8 legs in succession. This helped to fully validate the circuit and gait patterns. Because the motion patterns are preprogrammed into the switch case, it is imperative that

they work as intended. The experiment also served the secondary role of helping to calibrate the camera for use in the final experiment.

30 volts at 1 and 10 Hz were used for the multiple leg test. While 1 Hz is not very a practical frequency for the actual motion of the robot, it allowed the human eye to easily perceive the leg's motion and helped to troubleshoot errors in the gait patterns. The assembled legs can be seen in Fig 21.

5.2.2.3 Payload Test Results

During experimentation, we observed that when each leg was actuated individually, the payload was not moving. If, however, the actuators were paired and moved in a synchronized manner the payload experiences a larger actuation force, breaking static friction. The actuators were numbered and paired as shown in part C of Fig. 26. To achieve motion toward the left with respect to the ID mark individual legs were actuated in the sequence shown in part B of Fig. 26. There is a point where leg 3 is being disengaged and leg 1 is being engaged. The combined backward motion of leg 3 and forward motion of leg 1 creates double the net force of a single leg and is referred to as *Pair A* and marked in part C of Fig 26.

The gait sequence in Fig. 26 A can be further summarized as *Pair A*, *Pair B*, *Pair C*, then *Pair D* in that order. By changing the order of the sequence, the pairs can be reversed. For example, actuating leg 1 then releasing it while engaging leg 3 results in a backward motion of *Pair A*. By reversing all 4 *Pairs*, motion opposite to the prescribed sequence occurs which results in motion away from the ID mark. By re-ordering the sequence and leg actuation, one can achieve motion in any of the cardinal directions

similar to Fig. 12. The sequences shown in Table 4 show the input to displacement relationship observed during experimentation.

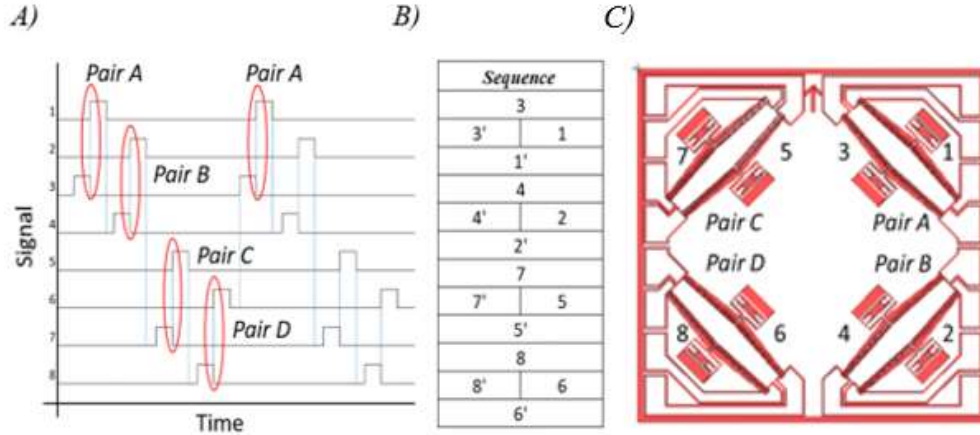


Figure 26. Shows the labelling and pairing of legs for SolarPede. A) Shows the gate sequence with pairs labeled. B) Shows the truth table for the legs to result in leftward motion of the payload. C) Shows the naming conventions of SolarPede legs.

Table 5.

Pair sequence where X indicates movement toward the outer edge of the substrate and X' indicates movement toward the interior of the substrate. A, B, C, and D correspond to Pairs shown in Fig 24. The direction of motion indicates payload travel with respect to the ID mark in Fig 24.

<i>Paired Leg Actuation Sequence</i>	<i>Direction of motion</i>	<i>Observed Displacement (over 10 seconds)</i>	<i>Observed Velocity</i>
A-B'-C-D'	UP	155 μm	15.5 $\mu\text{m/s}$
A'-B-C'-D	DOWN	121 μm	12.1 $\mu\text{m/s}$
A-B-C'-D'	LEFT	133 μm	13.3 $\mu\text{m/s}$
A'-B'-C-D	RIGHT	113 μm	11.3 $\mu\text{m/s}$
A'-B-C-D'	Rotate CW	-	3 mrad/s

SolarPede can also make its payload turn by setting half of the legs in reverse. By actuating any two pairs of legs that share an edge in the opposite direction of those on the other edge, rotation can be achieved as indicated in the results of Table 4, last row.

Vectors of motion can be seen in Fig. 12.

5.2.2 Solar Test Results

An experimental set up was assembled for tests with solar cells used as a power source for our SolarPede. Directed at this power source was a solar simulator from Newport Corporation, Irvine, USA, including a Xenon arching lamp (Newport 67005) with its power supply and controller (Newport 69907). The solar cell used in our tests had a size of ~ 20 mm x ~ 24 mm and was able to supply 3.3 V and 20 mA under standard conditions (sunlight). Upon exposure to the solar simulator's light, we can achieve higher currents by focusing the light and increasing its intensity. The setup for this experiment can be seen in Fig. 22.

5.2.2.1 General Power Output Results

We performed characterization of our solar cell, determining dependence of the supplied power by the cell on the power of the Xenon lamp. The light was applied to the cell and the output was measured using a multimeter. The resulting lamp power was recorded with the measured voltages and currents to produce the graph shown in Fig. 27.

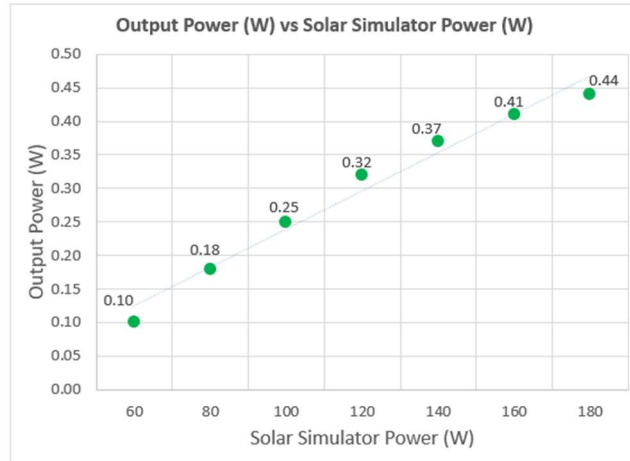


Figure 27. The X axis denotes the Solar Simulator input power and the Y axis denotes the output power from solar cell/input to the voltage booster.

Comparing the graph in Fig. 27 to the observed displacement vs input power of a single leg depicted in Fig. 24, we can conclude that at a range of 160 to 180 W light power on the solar simulator, the solar cell can generate microrobot power in excess of 0.33W. This produces a displacement between 6.46 μm and 14.21 μm for each microrobot leg.

5.2.2.2 Solar-Leg Results

Using the setup described in section 5.1.2.2, the full electronic backpack was tested under the operation of the SolarCell. Because the V2 board has components matched to its own design including an additional micro controller, the current draw and power consumption are higher than originally expected. While experiment results in section 5.2.2 show that the power available is .4 W at the output of the Voltage booster circuit, it is actually less with this experiment. Under the direct powering of the Solar Simulator, the Voltage booster output from the V2 board was +9.8 V at 21 mA, or .21 Watts. Combining this with displacement measurements shown in Fig. 24, a prediction

can be made that the displacement would be between 2 and 6 μm during actuation given the increased load from excess components. The actual value of the displacement was measured (using a camera) to be 3.5 μm which further validates the results in the previous sections and the given prediction. It also demonstrates the full operational capabilities of SolarPede when being powered by light. A closeup of the SolarPede leg can be seen below in Fig. 28.



Figure 28. Shows the SolarPede leg under high resolution camera.

CHAPTER 6

CONCLUSIONS AND FUTURE WORK

6.1 Conclusions

In this thesis is the analysis and experimental results that validate the untethered operation of SolarPede a novel light-powered micro-crawler. The microrobot body was fabricated using DRIE technology from SOI wafers with a cm^2 footprint. 8 Silicon legs were assembled into compliant socket connectors using a custom micro-assembly station in our lab. The leg layout on the microrobot body ensured that omni-directional 2D motions can be achieved using stick-and-slip of the leg on the substrate. An electronic backpack consisting of a Bluetooth enabled microcontroller, a solar cell, voltage booster, and power electronics was designed, and its components connected to the packaged body of the microrobot. In this configuration, locomotion was studied in the “belly-up” or conveyor configuration by placing a payload similar to the robot mass on top of the inverted legs. Experiments were conducted to verify that by multiplexing power between the actuators, the robot can achieve speeds of $13 \mu\text{m}/\text{second}$. Further experiments confirmed that the microrobot can be operated from an artificial light concentrator lamp.

With regard to the solar cell, which is not shown on the Electronic Backpack, provisions were made to mount this cell onto the board. As seen in Fig. 29, the top board features other unconnected terminals which could act as structural supports for the solar cell. The resulting design is shown in Fig 30 which is in essence, a three-board setup.

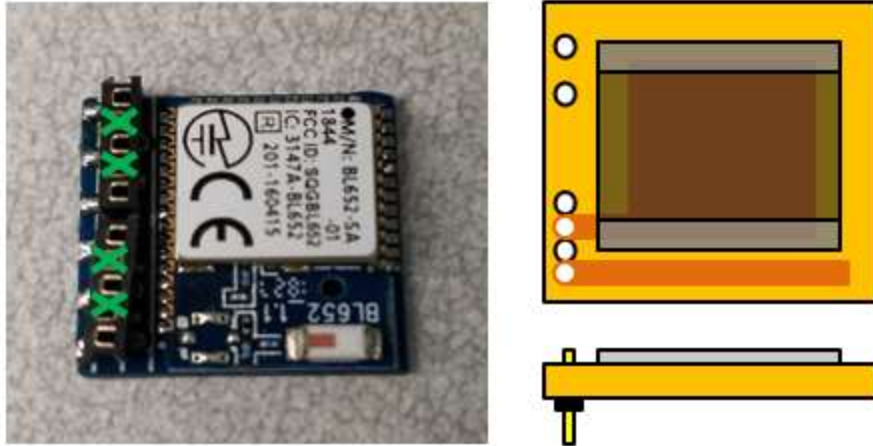


Figure 29. Shows the top board and proposed mating Solar Cell. X's mark unconnected terminals which would line up with through-holes shown in the right. The two copper colored holes near the bottom of the proposed board would be connected to ground and power.

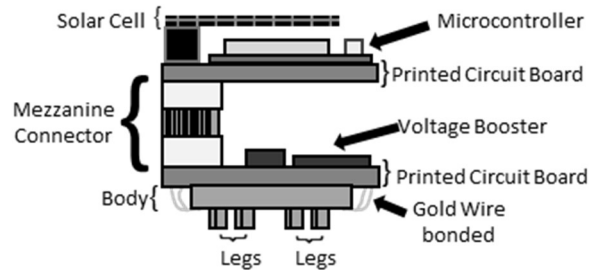


Figure 30. Shows the final system layout with the Solar Cell.

6.2 Future Work

In future work, the process of miniaturizing SolarPede continues. There are a number of ways to optimize the current design, but two are particularly attainable now that a testable module has been assembled. The first is to decrease the used footprint on SolarPede by removing the Mezzanine connector. One way to accomplish this is to replicate the ARRIPede design of having metal “pillars” support the weight of the top

board as shown below in Fig. 31. The drawback to this design is that the Microcontroller currently fills up the width of the footprint as can be seen in Fig. 15. It would be spatially challenging to place pins on either side of the controller without increasing the footprint or using supports too fragile to hold up the upper boards.

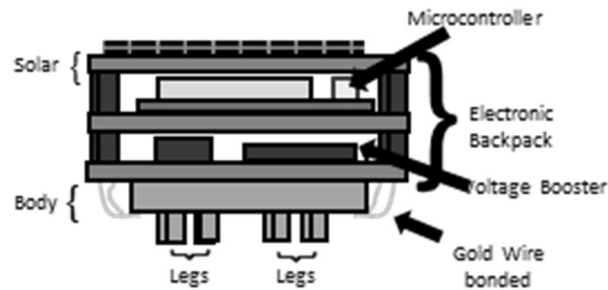


Figure 31. Shows a proposed shorter SolarPede backpack with easier assembly.

A second possibility for improving the design is to assemble the board on a Kapton Flex PCB. Flexible PCBs are a bit more expensive than their rigid counterparts but would feature a drastic decrease in weight. The proposed design can be seen in Fig. 32 with the total board shown on the left and two proposed assemblies on the right. The first uses a simple rod or screw. The second uses two small magnets which while not uncommon in Flex PCB designs, could cause interference. This board would also feature a small tab shown in the left as an extrusion from the right of the microcontroller. This extension could be clipped temporarily to an interface for programming.

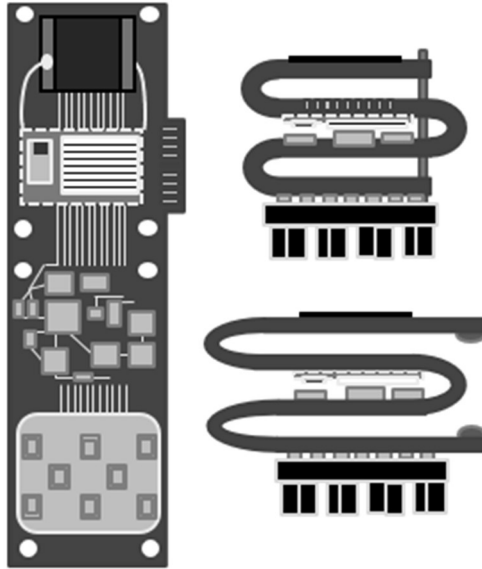


Figure 32. Shows a theoretical Flexible SolarPede made on bendable PCBs. This board design could be folded as shown on the right.

Improved PCB electronic backpacks will be implemented in the future. Like the current design, they will likely feature stacked double-sided boards with 15mm x 15mm form factors. Further testing with the existing SolarPede will continue with analysis of the stick-and-slip gaits during regular “belly down” operation. Finally, by combining an assembled SolarPede with a miniature robotic arm such as the sAFAM [4], mobile nano-scale manipulations may be accomplished.

REFERENCES

1. Chollet, Franck; Liu, Haobing. "A (not so) short introduction to MEMS" version 5.4, 2018.
2. Jaeger, Richard C. "Introduction to Microelectronic Fabrication" Addison-Wesley Longman Publishing Co., Inc., 1987.
3. Zhang, Ruoshi; Sherehiy, Andriy; Yang, Zhong; Wei, Danming; Harnett, Cindy K.; Popa, Dan O. "ChevBot – An Untethered Microrobot Powered by Laser for Microfactory Applications" in proceedings of International Conference on Robotics and Automation, Montreal 2019.
4. R. Zhang, D. Wei and D. O. Popa, "Design, Analysis and Fabrication of sAFAM, a 4 DoF Assembled Microrobot," 2018 International Conference on Manipulation, Automation and Robotics at Small Scales (MARSS), Nagoya, pp. 1-6, 2018.
5. Culpepper, Martin L.; Shih-Chi Chen. "Multiple degree of freedom micro electro-mechanical system positioner and actuator." U.S. Patent 7,451,596, issued November 18, 2008.
6. E. Blokhina et al., "Dielectric Charge Control in Electrostatic MEMS Positioners/Varactors," in Journal of Microelectromechanical Systems, vol. 21, no. 3, pp. 559-573, June 2012.
7. Ghafarian, Mohammadali; Shirinzadeh, Bijan; Al-Jodah, Ammar; Kumar Das, Tilok; Wei, Weichen; Tian, Yanling; Zhang, Dawei. "Design of a novel parallel monolithic 3-DOF compliant micromanipulator" in proceedings of Manipulation and Automation Robotics at Small Scales, Helsinki, Finland p8. 2019.
8. Hsu, Allen, Cregg Cowan, William Chu, Brian McCoy, Annjoe Wong-Foy, Ron Pelrine, Camilo Velez et al. "Automated 2D micro-assembly using diamagnetically levitated milli-robots." In 2017 international conference on manipulation, automation and robotics at small scales (MARSS), pp. 1-6. IEEE, 2017.
9. Pelrine, Ron; Hsu, Allen; Wong-Foy, Annjoe. "Methods and Results for Rotation of Diamagnetic Robots Using Translational Designs" in proceedings of Manipulation and Automation Robotics at Small Scales, Helsinki, Finland p45. 2019.
10. Legtenberg, Rob; Groenveld, A. W.; Elwenspoek M. "Comb-drive actuators for large displacements." Journal of Micromechanics and Microengineering, 1996.
11. Yan, Dong. "Mechanical design and modeling of MEMS thermal actuators for RF applications." Diss. University of Waterloo, 2002.

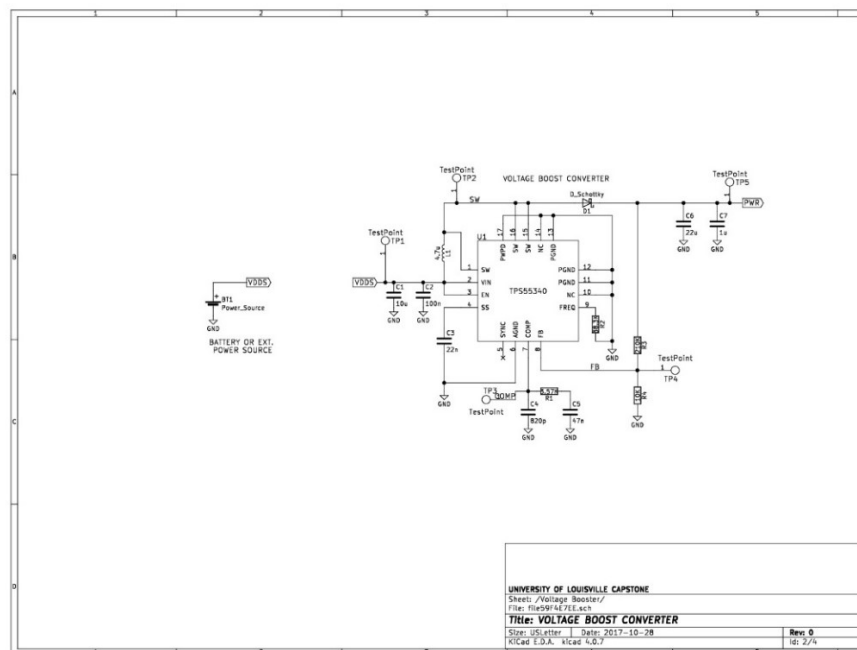
12. Varona, Jorge, Margarita Tecpoyotl-Torres, and Anas A. Hamoui. "Design of MEMS vertical–horizontal chevron thermal actuators." *Sensors and actuators A: Physical* 153.1, 127-130, 2009.
13. Bell, Dominik J.; Lu, T J; Fleck, N A; Spearing, S M. "MEMS actuators and sensors: observations on their performance and selection for purpose." *Journal of Micromechanics and Microengineering* 15.7, S153, 2005.
14. D. R. Frutiger; B. E. Kratochvil; Bradley J. Nelson. "MagMites - Microrobots for Wireless Microhandling in Dry and Wet Environments" in proceedings of ICRA 2010, Anchorage Alaska, 2010.
15. D. R. Frutiger; K. Vollmers; B. E. Kratochvil; Bradley J. Nelson. "Small, Fast, and Under Control: Wireless Resonant Magnetic Micro-agents" in *The International Journal of Robotics Research* Vol. 29, No. 5, pp. 613-636, 2010.
16. Nam, Jackwang, Seungmun Jeon, Seungjoo Kim, and Gunhee Jang. "Crawling microrobot actuated by a magnetic navigation system in tubular environments." *Sensors and Actuators A: Physical* 209, p100-106, 2014.
17. Menon, Carlo, and Metin Sitti. "Biologically inspired adhesion based surface climbing robots." *Proceedings of the 2005 IEEE International Conference on Robotics and Automation*. IEEE, 2005.
18. Abbot, Jake J.; Nagy, Zoltán; Beyeler, Felix; Nelson, Bradley J. "Robotics in the Small" in *IEEE Robotics and Automation Magazine* 1070-9932/07 pp. 92-103 (2007).
19. H. Woern, M. Szymanski and J. Seyfried, "The I-SWARM project," *ROMAN 2006 - The 15th IEEE International Symposium on Robot and Human Interactive Communication*, Hatfield, pp. 492-496. 2006
20. Caprari, Gilles, and Roland Siegwart. "Mobile micro-robots ready to use: Alice." *2005 IEEE/RSJ international conference on intelligent robots and systems*. IEEE, 2005.
21. Ebefors, Thorbjörn, et al. "A walking silicon micro-robot." *Proc. Transducers' 99*. 1999.
22. R. Murthy and D. O. Popa, "Millimeter-scale microrobots for wafer-level factories," in *Proceedings of 2010 IEEE International Conference on Robotics and Automation*, Anchorage, AK, pp. 488-493, 2010.
23. Jafferis, Noah T., et al. "Untethered flight of an insect-sized flapping-wing microscale aerial vehicle." *Nature* 570.7762, 491, 2019.
24. T. Fukuda and H. Ishihara, "Micro optical robotic system with cordless optical power supply," *Proceedings of 1993 IEEE/RSJ International Conference on Intelligent Robots and Systems (IROS '93)*, Yokohama, Japan, 1993, pp. 1703-1708 vol.3.
25. Maslen, Charlie; Eral, H. Burak; Stepanek, Frantisek; Cigler, Petr; Rehor, Ivan. "Hydrogel Microcrawlers Self-Assembly into Ordered Solid Sheets of Unable Geometry*" in proceedings of *Manipulation and Automation Robotics at Small Scales*, Helsinki, Finland p84. 2019.

26. Chang, Kenneth. "The Microbots Are on Their Way" New York Times, Molecular Machines pD2, 2019.
27. Rubenstein, Michael, Christian Ahler, and Radhika Nagpal. "Kilobot: A low cost scalable robot system for collective behaviors." 2012 IEEE International Conference on Robotics and Automation. IEEE, 2012.
28. Hofmann, Andreas, et al. "Evolvable Micro Production Systems: Specific needs and differences to macro." 2011 IEEE International Symposium on Assembly and Manufacturing (ISAM). IEEE, 2011.
29. Seyfried, J., et al. "Controlling cm³ Sized Autonomous Micro Robots Operating in the Micro and Nano World." Proc. Int. Conf. on Climbing and Walking Robots and their Supporting Technologies (CLAWAR'03). 2003.Desktop Factories
30. Pérez, Roberto, et al. "Reconfigurable micro-machine tool design for desktop machining micro-factories." IFAC Proceedings Volumes 46.9 (2013): 1417-1422.
31. Zhang, Xiang, Cheng Sun, and Nicholas Fang. "Manufacturing at nanoscale: Top-down, bottom-up and system engineering." Journal of Nanoparticle Research 6.1 (2004): 125-130.
32. Honegger, Andrew E., et al. "Development of an Automated Microfactory: Part 1—Microfactory Architecture And Sub-Systems Development." (2006).
33. Honegger, Andrew E., et al. "Development of an automated microfactory: part 2—experimentation and analysis." Trans. North Am. Manuf. Res. Inst. SME. 2006.
34. A. Hsu, C. Cowan, W. Chu, B. McCoy, A. Wong-Foy, R. Pelrine and C. Velez, "Automated 2D micro-assembly using diamagnetically levitated milli-robots," in Proceedings of 2017 IEEE International Conference on Manipulation, Automation and Robotics at Small Scales (MARSS), pp. 1-6, 2017.
35. R. Murthy, A.N. Das, D.O. Popa and H.E. Stephanou ARRIpede, "An Assembled Die-Scale Microcrawler", in Advanced Robotics, 25:8, pp. 965-990, 2011.
36. R. Murthy, A.N. Das and D.O. Popa. "Nonholonomic Control for an Assembled Microcrawler," in IFAC Proceedings Volumes 42, no. 16 pp. 627-632, 2009.
37. Power Electronics for Assembled Microrobots Final Report Prepared by Bryan Knight, David Le, and James Simmons. 12/05/2017 Rev 0
38. Texas Instruments, "Integrated 5-A Wide Input Range Boost/SEPIC/Flyback DC/DC Regulator datasheet (Rev. D)," TPS55340 datasheet (Rev D), 2012 (Revised 2019)
39. Power Electronics for "ARRIpede: An Assembled Micro Crawler" prepared by Madison Buechler, Jordan Klotz, and Justin Tran. 4/15/2018 Rev 1
40. HIROSE ELECTRIC CO, "10+ Gbps 0.8mm pitch Board-to-Board Connectors" ER8 Series datasheet (rev 3) 2017, (Revised 2019)
41. Klotz, Jordan; Wei, Danming; Yang, Zhong; Sherehiy, Andriy; Saadatzi, Mohammad N.; Zhang, Ruoshi; Popa, Dan O. "Concept Validation for a Novel Stick-and-Slip, Light-Powered, Mobile Micro-Crawler" in proceedings of Manipulation and Automation Robotics at Small Scales, Helsinki, Finland p81. 2019.

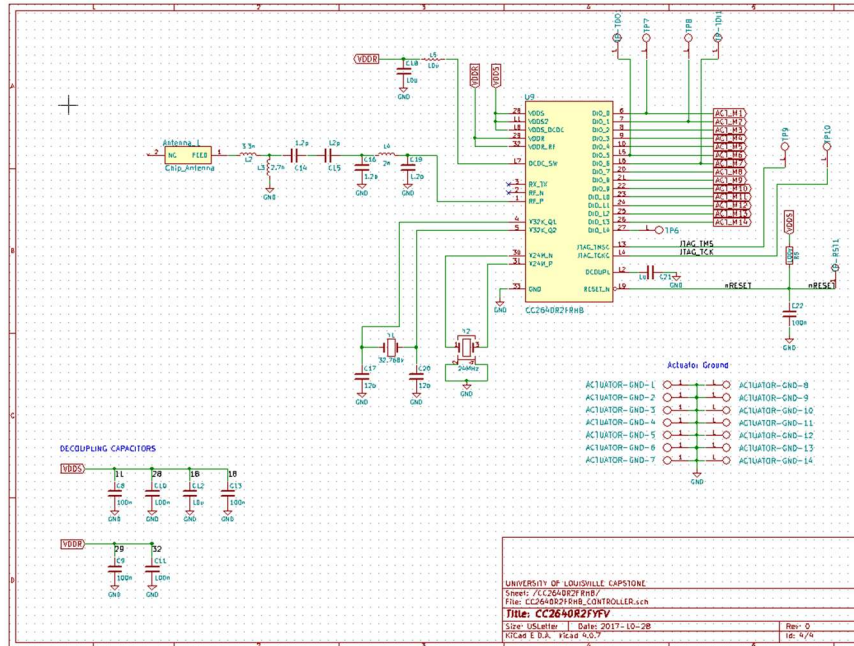
42. Diodes Incorporated, "N-Channel Enhancement Mode MOSFET" DMN62D0U datasheet (Rev 2), 2016.
43. Moro, Shashank U. "Wifi enabled smart robot." Science, Engineering and Technology Conference, At VIT University, Vellore. 2013.
44. Ebert, Julia T., Melvin Gauci, and Radhika Nagpal. "Multi-feature collective decision making in robot swarms." Proceedings of the 17th International Conference on Autonomous Agents and MultiAgent Systems. International Foundation for Autonomous Agents and Multiagent Systems, 2018.
45. Hilder, James, et al. "The Psi Swarm: A low-cost robotics platform and its use in an education setting." Annual Conference Towards Autonomous Robotic Systems. Springer, Cham, 2016.
46. Corradi, Paolo, et al. "Optical networking in a swarm of microrobots." International Conference on Nano-Networks. Springer, Berlin, Heidelberg, 2008.
47. Arvin, Farshad, et al. "Colias: An autonomous micro robot for swarm robotic applications." International Journal of Advanced Robotic Systems 11.7 (2014): 113.
48. Ferranti, Ludovico, and Francesca Cuomo. "Nano-wireless communications for microrobotics: An algorithm to connect networks of microrobots." Nano communication networks 12 (2017): 53-62.
49. Gauci, Melvin, et al. "Error cascades in collective behavior: a case study of the gradient algorithm on 1000 physical agents." Proceedings of the 16th Conference on Autonomous Agents and MultiAgent Systems. International Foundation for Autonomous Agents and Multiagent Systems, 2017.
50. Boillot, Nicolas, Dominique Dhoutaut, and Julien Bourgeois. "Using nano-wireless communications in micro-robots applications." Proceedings of ACM the first annual international conference on nanoscale computing and communication. ACM, 2014.
51. Ferranti, Ludovico, and Francesca Cuomo. "Nano-wireless Communication for Microrobotics: bridging the gap." Proceedings of the Second Annual International Conference on Nanoscale Computing and Communication. ACM, 2015.
52. Laird Connectivity, "BL652 Series – Bluetooth v5 +NFC" BL652 datasheet (V 2.9), 2019.
53. Laird Connectivity, "User Guide, *smart*BASIC Core Functionality" Version 3.0, 2018.
54. Laird Connectivity, "User Guide, BL652 *smart*BASIC Extensions" release 28.9.5.0, 2018.
55. Shay, Byron, Ted Hubbard, and Marek Kujath. "Linear frictional micro-conveyors." Sensors and Actuators A: Physical 148.1 (2008): 290-

APPENDIX A

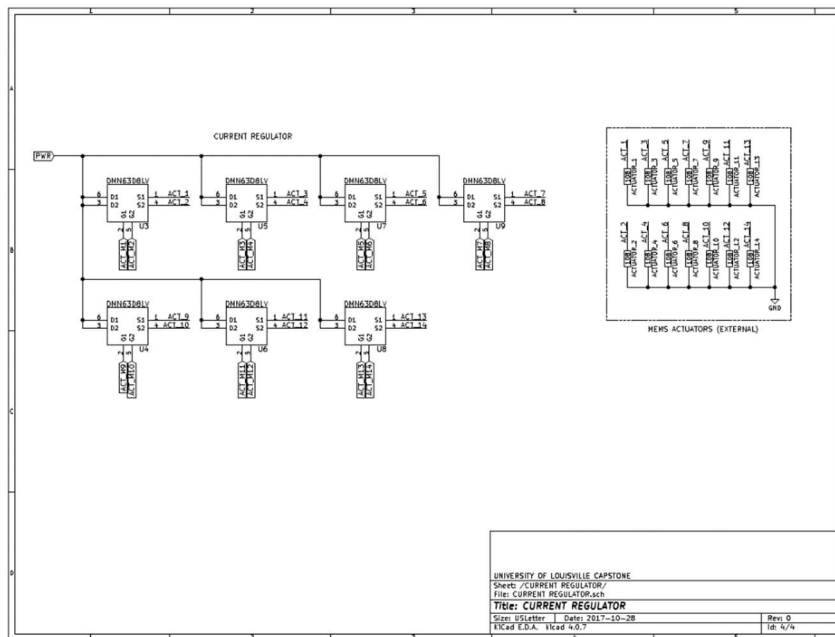
Appendix A contains all of the circuits for the various generations of Electronic Backpacks which are referenced in the text. The included designs show only the finished product and not the various revisions which were made during the life of the different projects. It should be noted that the author was responsible for the creation of all schematics for the ARRIPede V3 and after. Additionally, the author converted the ARRIPede V2 schematics from their original state in KiCAD to Eagle for ease of use in future designs though those are not shown in APPENDIX A.



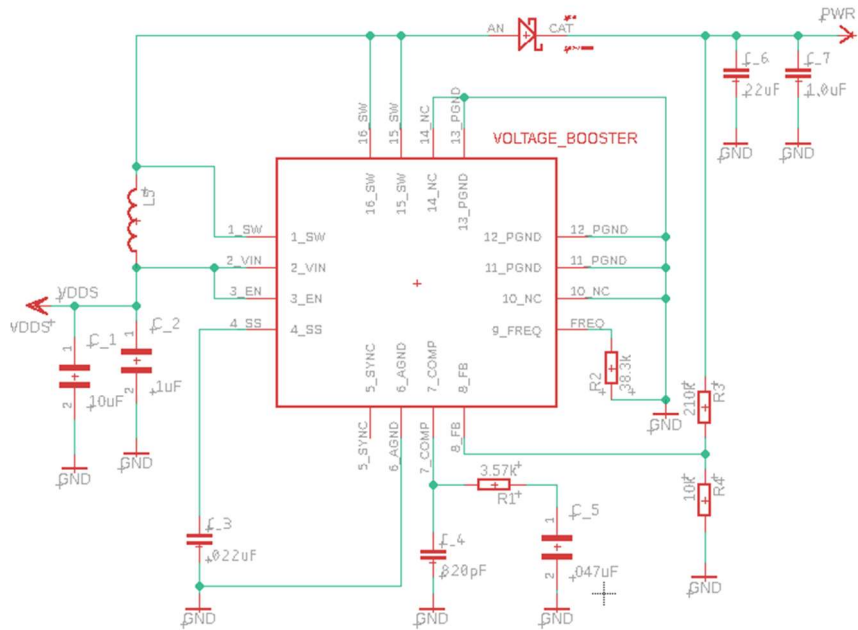
Shows the Voltage Booster schematic from ARRIPede V2 as created in KiCAD.



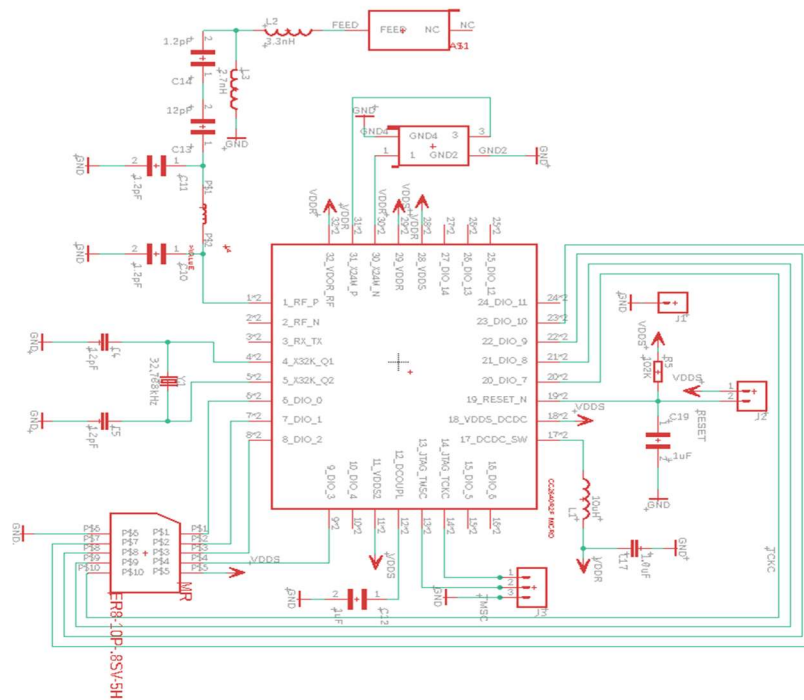
Shows CC2640 Microcontroller schematic from the ARRIPede V2 as created using KiCAD.



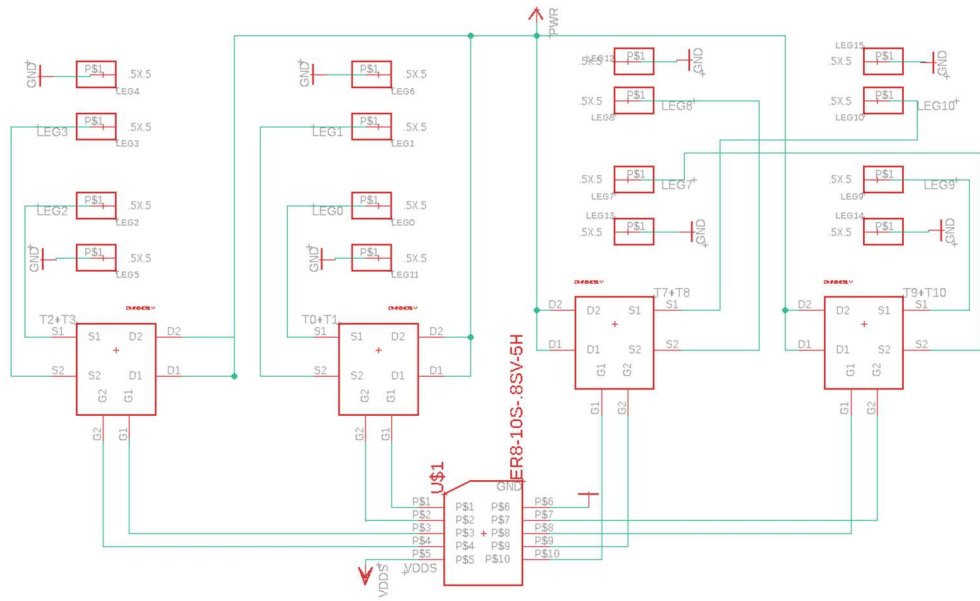
Shows the Transistor Array schematic from the ARRIPede V2 as created using KiCAD.



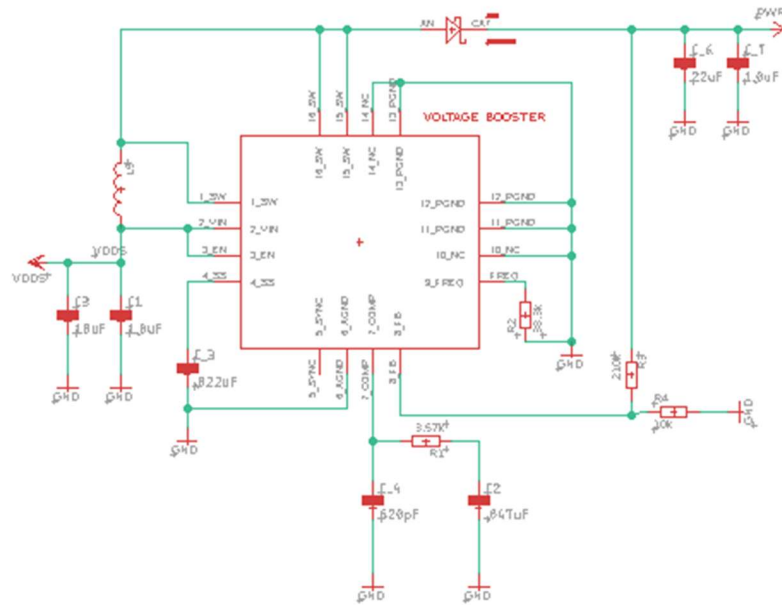
Shows the Voltage Booster Schematic for the ARRIPede V3 as created using EagleCAD.



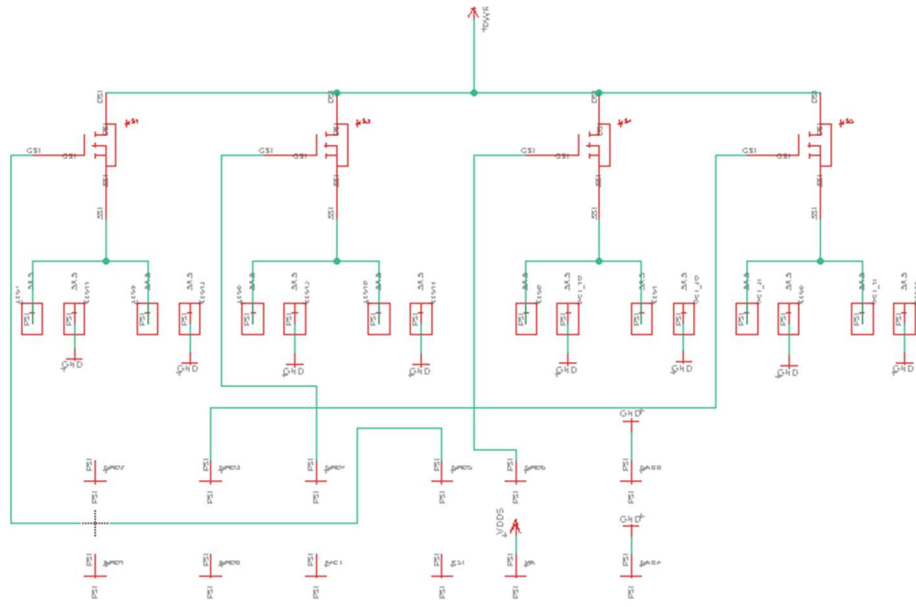
Shows the CC2640 and Antenna Schematic for the ARRIPede V3 as created using EagleCAD.



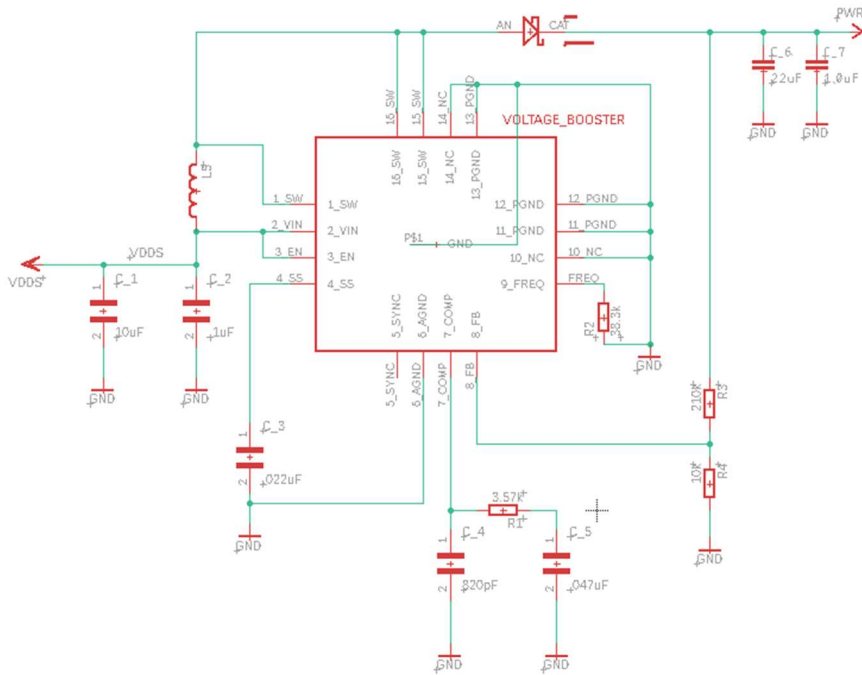
Shows Transistor Array and Mezzanine schematic for ARRIPede V3 as created using EagleCAD.



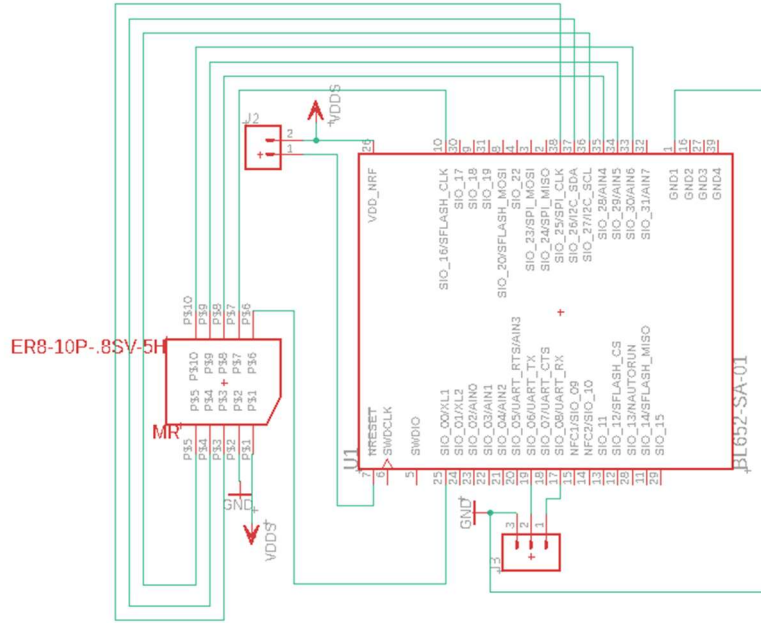
Shows Voltage Booster Schematic for SolarPede V0 as created using EagleCAD



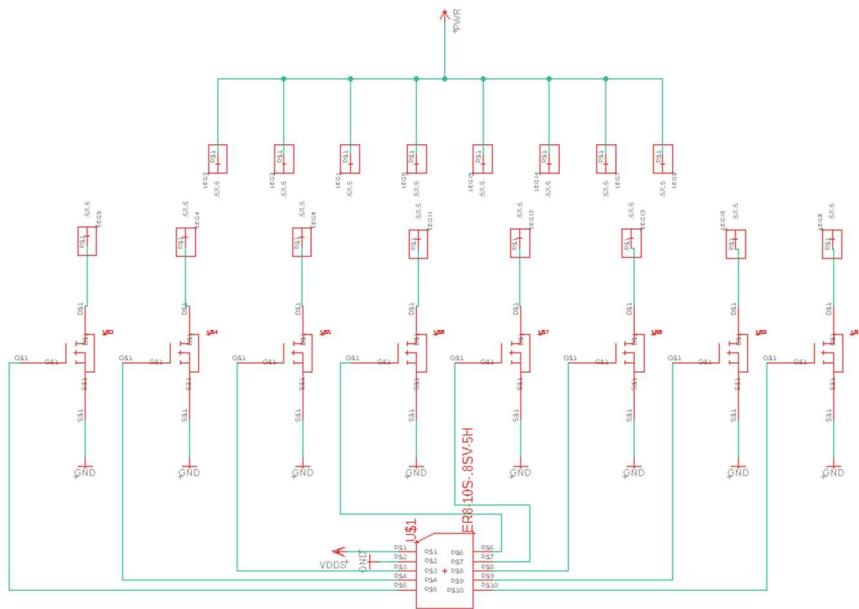
Shows Transistor Array and castellated through holes for SolarPede V0 as created using EagleCAD. Additional unwired connectors were designed to increase structural integrity of the Electronic Backpack.



Shows the Voltage Booster Schematic for SolarPede V1 as created using EagleCAD



Shows the BL652 and Mezzanine connector as created using EagleCAD. BL652 footprint and symbol taken from Laird Connectivity resources for BL652 wireless module.



Shows the Transistor Array and wire-bonding pads for SolarPede V1 as created using EagleCAD.

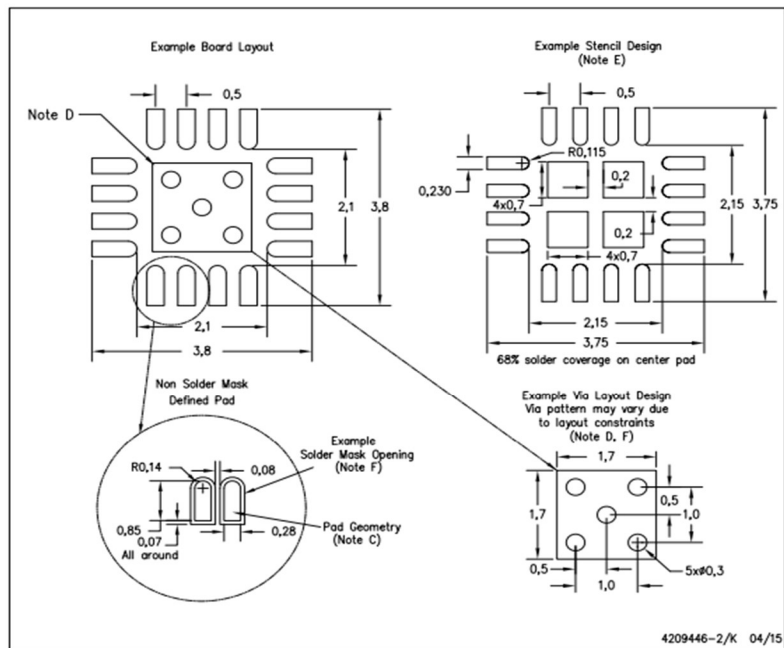
APPENDIX B

Appendix B holds excerpts from the datasheets for components which were used in the manufacture of SolarPede V1. In particular, it contains the PCB footprints of the components used to make the custom library elements used during the Electronic Design Process.

Voltage Booster Footprint [38]

LAND PATTERN DATA

RTE (S-PWQFN-N16) PLASTIC QUAD FLATPACK NO-LEAD



- NOTES:
- All linear dimensions are in millimeters.
 - This drawing is subject to change without notice.
 - Publication IPC-7351 is recommended for alternate designs.
 - This package is designed to be soldered to a thermal pad on the board. Refer to Application Note, Quad Flat-Pack Packages, Texas Instruments Literature No. SLUA271, and also the Product Data Sheets for specific thermal information, via requirements, and recommended board layout. These documents are available at www.ti.com.
 - Laser cutting apertures with trapezoidal walls and also rounding corners will offer better paste release. Customers should contact their board assembly site for stencil design recommendations. Refer to IPC 7525 for stencil design considerations.
 - Customers should contact their board fabrication site for minimum solder mask web tolerances between signal pads.

Transistor Footprints [42]

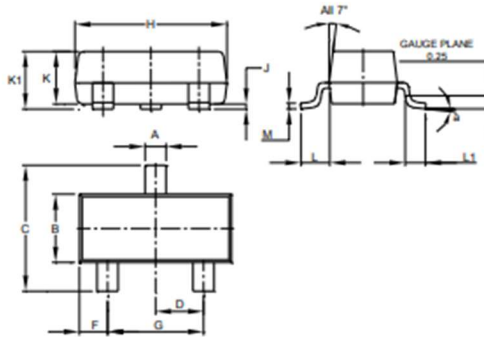


DMN62D0U

Package Outline Dimensions

Please see <http://www.diodes.com/package-outlines.html> for the latest version.

SOT23

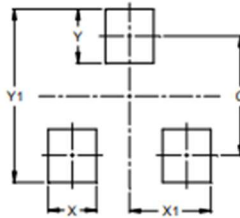


SOT23			
Dim	Min	Max	Typ
A	0.37	0.51	0.40
B	1.20	1.40	1.30
C	2.30	2.50	2.40
D	0.89	1.03	0.915
F	0.45	0.60	0.535
G	1.78	2.05	1.83
H	2.80	3.00	2.90
J	0.013	0.10	0.05
K	0.890	1.00	0.975
K1	0.903	1.10	1.025
L	0.45	0.61	0.55
L1	0.25	0.55	0.40
M	0.085	0.150	0.110
a	0°	8°	---
All Dimensions in mm			

Suggested Pad Layout

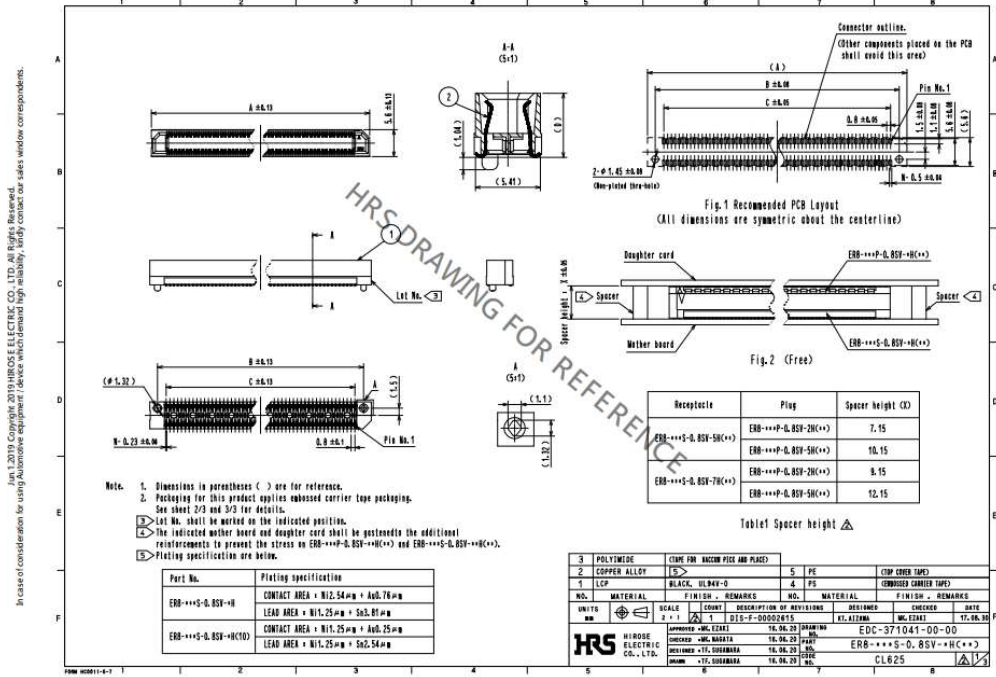
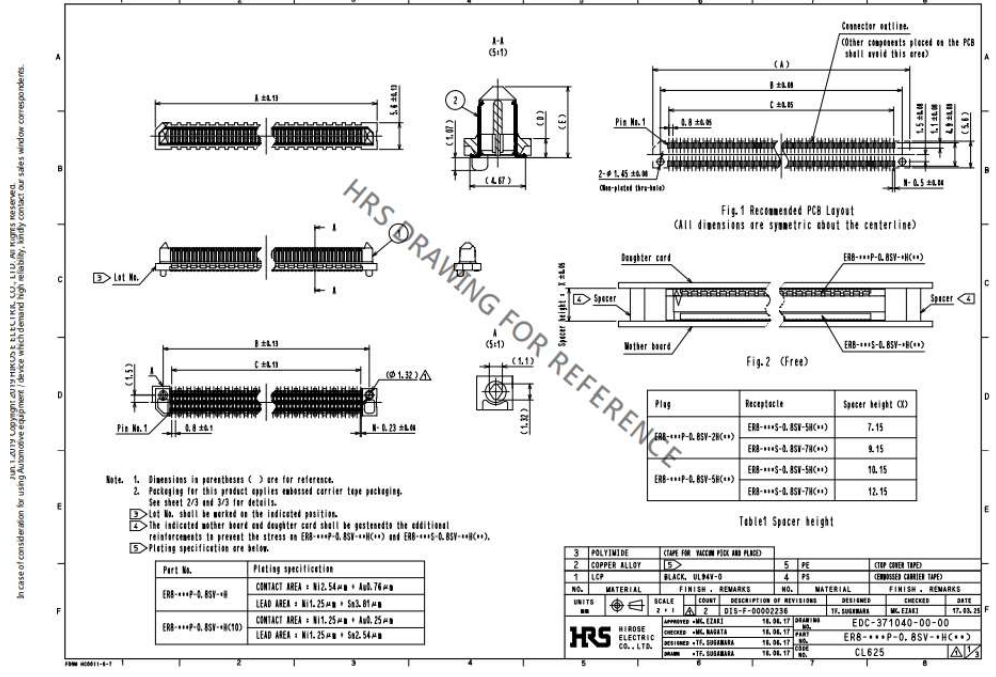
Please see <http://www.diodes.com/package-outlines.html> for the latest version.

SOT23



Dimensions	Value (in mm)
C	2.0
X	0.8
X1	1.35
Y	0.9
Y1	2.9

ER8 Mezzanine Connectors [40]



APPENDIX C

This section includes code used for modelling the response of SolarPede in MATLAB and the *smart*BASIC code used for the generation of gait sequences during the experimentation of SolarPede. All code font sizes reduced to help with spacing.

*smart*BASIC program for single leg actuation.

```
DIM rc,i,wait,leg as integer

leg = 16
rc = gpiofuncsetfunc(leg,2,0)
//Delay Subroutine
wait = 1000
SUB delay(ms)
dim i : i = GetTickCount()
while GetTickCountSince(i)<ms
endwhile
ENDSUB

for i=1 to 10
print "\nLeg On\n"
gpiowrite(leg,1) //Turn leg 1 on
delay(30000) //Delay for actuation
gpiowrite(leg,0) //Turn leg 1 off
print "\nLeg Off\n"
delay(wait) //Set next leg
next
```

*smart*BASIC program for operation under UART connection. Used in Payload experiments and acts as a basis for future development.

```
//+++++
//Variable initialization and leg assignment
// ^ Front ^
// 1(28) 2(28)
// 3(26) 4(29)
// 5(14) 6(30)
// 7(16) 8(31)
DIM rc //Used for set functions
DIM leg1,leg2,leg3,leg4,leg5,leg6,leg7,leg8,gait,wait
leg1=16 //io chosen from free pins on devkit
leg2=16
leg3=27
leg4=29
leg5=14
leg6=30
```

```

leg7=29
leg8=31
rc = gpiofunc(leg1,2,0)
rc = gpiofunc(leg2,2,0)
rc = gpiofunc(leg3,2,0)
rc = gpiofunc(leg4,2,0)
rc = gpiofunc(leg5,2,0)
rc = gpiofunc(leg6,2,0)
rc = gpiofunc(leg7,2,0)
rc = gpiofunc(leg8,2,0)
//+++++

//+++++
//Delay Subroutine
wait = 250
SUB delay(ms)
dim i : i = GetTickCount()
while GetTickSince(i)<ms
endwhile
ENDSUB
//+++++
//+++++
//Exit Subroutine
SUB Exit()
reset(0)
ENDSUB
//+++++

//+++++
DIM hMyChar, count
//=====
// Initialise and instantiate service, characteristic,
//=====
FUNCTION OnStartup()
    DIM rc, hSvc, attr$ : attr$="Forward"
    //commit service
        rc = BleServiceNew(1, BleHandleUuid16(0x18EE), hSvc)
    //initialise char, write/read enabled, accept signed writes
    rc=BleCharNew(0x4A,BleHandleUuid16(1),BleAttrMetaData(1,1,20,0,rc),0,0)
    //commit char initialised above, with initial value "forward" to service 'hSvc'
    rc=BleCharCommit(hSvc,attr$,hMyChar)
    //commit changes to service
    rc = BleServiceCommit(hSvc)
ENDFUNC rc

//=====
// Uart Rx handler - write input to characteristic
//=====
FUNCTION Starter()
    TimerStart(0,10,0)
ENDFUNC 1

//=====
// Timer0 timeout handler
//=====
FUNCTION Movement()
    DIM t$ : rc=UartRead(t$)
    rc = BleCharValueWrite(hMyChar,t$)
    IF rc==0 THEN
        PRINT "\nYou just ran ";t$;"type another listed option or type complete to
exit\n"
    WHILE count <10
    IF strlen(t$) == 8 THEN //1 represents forward
        gpiowrite(leg1,1) //Turn leg 1 on
        delay(wait) //Delay for actuation
        gpiowrite(leg1,0) //Turn leg 1 off
        delay(wait)
        gpiowrite(leg1,1) //Turn leg 1 on
        delay(wait) //Delay for actuation
        gpiowrite(leg1,0) //Turn leg 1 off
        delay(wait)
    
```

```

gpiowrite (leg1,1) //Turn leg 1 on
delay(wait) //Delay for actuation
gpiowrite (leg1,0) //Turn leg 1 off
delay(wait)
gpiowrite (leg1,1) //Turn leg 1 on
delay(wait) //Delay for actuation
gpiowrite (leg1,0) //Turn leg 1 off
delay(wait)
gpiowrite (leg1,1) //Turn leg 1 on
delay(wait) //Delay for actuation
gpiowrite (leg1,0) //Turn leg 1 off
delay(wait)
gpiowrite (leg1,1) //Turn leg 1 on
delay(wait) //Delay for actuation
gpiowrite (leg1,0) //Turn leg 1 off
delay(wait)
gpiowrite (leg1,1) //Turn leg 1 on
delay(wait) //Delay for actuation
gpiowrite (leg1,0) //Turn leg 1 off
//
elseif strlen(t$) == 6 THEN //2 represents LEFT turn
gpiowrite (leg1,1)
delay(wait)
gpiowrite (leg1,0)
gpiowrite (leg2,1)
delay(2*wait)
gpiowrite (leg2,0)
gpiowrite (leg3,1)
delay(wait)
gpiowrite (leg3,0)
gpiowrite (leg4,1)
delay(2*wait)
gpiowrite (leg4,0)
gpiowrite (leg5,1)
delay(wait)
gpiowrite (leg5,0)
gpiowrite (leg6,1)
delay(2*wait)
gpiowrite (leg6,0)
gpiowrite (leg7,1)
delay(wait)
gpiowrite (leg7,0)
gpiowrite (leg8,1)
delay(2*wait)
gpiowrite (leg8,0)
//
elseif strlen(t$) == 7 THEN //3 represents RIGHT turn
gpiowrite (leg1,1)
delay(2*wait)
gpiowrite (leg1,0)
gpiowrite (leg2,1)
delay(wait)
gpiowrite (leg2,0)
gpiowrite (leg3,1)
delay(2*wait)
gpiowrite (leg3,0)
gpiowrite (leg4,1)
delay(wait)
gpiowrite (leg4,0)
gpiowrite (leg5,1)
delay(2*wait)
gpiowrite (leg5,0)
gpiowrite (leg6,1)
delay(wait)
gpiowrite (leg6,0)
gpiowrite (leg7,1)
delay(2*wait)
gpiowrite (leg7,0)
gpiowrite (leg8,1)
delay(wait)
gpiowrite (leg8,0)

```

```

elseif strlen(t$) == 5 THEN //Stop or idle
gpiowrite(leg1,0)
gpiowrite(leg2,0)
gpiowrite(leg3,0)
gpiowrite(leg4,0)
gpiowrite(leg5,0)
gpiowrite(leg6,0)
gpiowrite(leg7,0)
gpiowrite(leg8,0)
elseif strlen(t$) == 9 THEN
gpiowrite(leg1,0)
gpiowrite(leg2,0)
gpiowrite(leg3,0)
gpiowrite(leg4,0)
gpiowrite(leg5,0)
gpiowrite(leg6,0)
gpiowrite(leg7,0)
gpiowrite(leg8,0)
PRINT "exiting"
exit()
else
gpiowrite(leg1,0)
gpiowrite(leg2,0)
gpiowrite(leg3,0)
gpiowrite(leg4,0)
gpiowrite(leg5,0)
gpiowrite(leg6,0)
gpiowrite(leg7,0)
gpiowrite(leg8,0)
print "Not a valid option\n"
ENDIF
count = count+1
ENDWHILE
ELSE
PRINT "\nFailed to write new gate option ";integer.h'rc;"\n"
ENDIF
gpiowrite(leg1,0)
gpiowrite(leg2,0)
gpiowrite(leg3,0)
gpiowrite(leg4,0)
gpiowrite(leg5,0)
gpiowrite(leg6,0)
gpiowrite(leg7,0)
gpiowrite(leg8,0)
count = 1
ENDFUNC 0

FUNCTION DelaySet()
DIM count
DIM t$ : rc=UartRead(t$)
rc = BleCharValueWrite(hMyChar,t$)
IF rc==0 THEN
wait = strvaldec(t$)
PRINT "\Delay set to ";t$;" ms"
ELSE
PRINT "\nFailed to write new gate option ";integer.h'rc;"\n"
ENDIF
ENDFUNC 2

SUB BleGaitSelect()
IF OnStartup()==0 THEN
DIM at$ : rc = BleCharValueRead(hMyChar,at$)
PRINT "\nPlease make a selection or type complete\n"
ELSE
DIM ab$ : rc = BleCharValueRead(hMyChar,ab$)
PRINT "\n"
ENDIF

ONEVENT EVUARTRX CALL Starter

```

```

ONEVENT EVTMR0          CALL Movement

WAITEVENT
ENDSUB
//+++++
//+++++
//Gait Patterns and case
PRINT "\nThe Most recent gait was: Forward\nType one of the
following\nforward,tleft,tright,idle\n"
WHILE gait < 20
BleGaitSelect()
count = 0
gait=gait+1
ENDWHILE
//+++++

```

MATLAB code used in the modelling of SolarPede including transfer function and step response generation.

```

clc;
clear;
H_absorb = .05e-6
H_conduct = 20e-6 % H_absorb
tau_Si = 20e-6
W = 10000e-6
L = 10000e-6
H = 1000e-6
rho_Si = 2330
rho_Air = 1.225
resistivity_Si = 0.02
h_Air = 10
k_Air = 0.025
k_Si = 124
c_Air = 716
c_Si = 702
tau_Air = 10e-6
Length_Si_pad = 10000e-6
T_env = 20
reflectivity = 0.3
absorption = 7.85e3

L_beam = sqrt((2000e-6)^2+(120e-6)^2)
beta = atan(120/2000) %2.86 degree
%beta = 2.86
alpha_Si = 2.6e-6
%resistivity_Si = 0.0001 %ohm m
N=6
young_s_modulus = 169e9
A_cross = 100e-6*12e-6
%theta = 2.86%0.04991642
theta = beta
mu = 0.35
mu_s_1 = 0.4
mu_d_1 = 0.33
mu_s_2 = 0.4
mu_d_2 = 0.33
alpha = 0.0872665

inital_dx1 = 0
inital_x1 = 0
inital_dx2 = 0
inital_x2 = 200e-6
inital_dPhi = 0
inital_Phi = 0

```

```
theta1 = 1.5708
theta2 = -1.5708

resistance_power = 0.27

b = 0.1
k_actuator = 185

m = L*W*tau_Si*rho_Si
m1 = 3e-7
m2 = 2.5e-4
% m1 = 0.1*m
% m2 = 0.9*m
% m1 = m/8
% m2 = 0.1*m1
angular_inertia = m*(W^2+L^2)/12
I0 = 200e-6

r1 = 4000e-6
r2 = 4000e-6
```

CURRICULUM VITA

NAME: Jordan Fredrick Klotz
ADDRESS: NGS-SRB Lab
Shumaker Research Building 213
2210 S Brook St,
Louisville, KY 40208
DOB: Elizabethtown, Kentucky – April 8, 1997

EDUCATION
& TRAINING: B.S. Electrical Engineering
J. B. Speed School of Engineering, University of Louisville
2014-2018

PUBLICATIONS: First author for “Concept Validation for a Novel Stick-and-Slip,
Light-Powered, Mobile Micro-Crawler” Submitted to MARSS
2019 in Helsinki, Finland.

PRESENTATIONS: Poster Presentation at Spring Undergraduate Research and
Community Engagement Symposium 2018 at University of
Louisville, KY
Full Paper presentation at International Conference on
Manipulation, Automation and Robotics at Small Scales (MARSS)
2019 in Helsinki, Finland.
Poster Presentation at 2019 KY Nano+AM Symposium at
University of Louisville, KY

AWARDS: Scientific Research Poster Award at 2019 KY Nano+AM
Symposium at University of Louisville, KY